Chapter 5

Chemical sediments associated with Neoproterozoic glaciation: iron formation, cap carbonate, barite and phosphorite

PAUL F. HOFFMAN[1,2] *, FRANCIS A. MACDONALD[1] & GALEN P. HALVERSON[3,4]

[1]*Department of Earth and Planetary Sciences, Harvard University, 20 Oxford Street, Cambridge, MA, 02138, USA*

[2]*School of Earth and Ocean Sciences, University of Victoria, Box 1700, Victoria, BC V6W 2Y2, Canada*

[3]*School of Earth and Environmental Sciences, The University of Adelaide, North Terrace, Adelaide, SA 5005, Australia*

[4]*Present address: Department of Earth and Planetary Sciences, McGill University, 3450 University Street, Montréal, PQ H3A 2K6, Canada*

**Corresponding author (e-mail: paulfhoffman@yahoo.com)*

Abstract: Orthochemical sediments associated with Neoproterozoic glaciation have prominence beyond their volumetric proportions because of the insights they provide on the nature of glaciation and the records they hold of the environment in which they were precipitated. Synglacial Fe formations are mineralogically simple (haematite jaspilite), and their trace element spectra resemble modern seawater, with a weaker hydrothermal signature than Archaean–Palaeoproterozoic Fe formations. Lithofacies associations implicate subglacial meltwater plumes as the agents of Fe(II) oxidation, and temporal oscillations in the plume flux as the cause of alternating Fe- and Mn-oxide deposits. Most if not all Neoproterozoic examples belong to the older Cryogenian (Sturtian) glaciation. Older and younger Cryogenian (Marinoan) cap carbonates are distinct. Only the younger have well-developed transgressive cap dolostones, which were laid down during the rise in global mean sea level resulting from ice-sheet meltdown. Marinoan cap dolostones have a suite of unusual sedimentary structures, indicating abnormal palaeoenvironmental conditions during their deposition. Assuming the meltdown of ice-sheets was rapid, cap dolostones were deposited from surface waters dominated by buoyant glacial meltwater, within and beneath which microbial activity probably catalysed dolomite nucleation. Former aragonite seafloor cement (crystal fans) found in deeper water limestone above Marinoan cap dolostones indicates carbonate oversaturation at depth, implying extreme concentrations of dissolved inorganic carbon. Barite is associated with a number of Marinoan cap dolostones, either as digitate seafloor cement associated with Fe-dolomite at the top of the cap dolostone, or as early diagenetic void-filling cement associated with tepee or tepee-like breccias. Seafloor barite marks a redoxcline in the water column across which euxinic Ba-rich waters upwelled, causing simultaneous barite titration and Fe(III) reduction. Phosphatic stromatolites, shrub-like structures and coated grains are associated with a glacioisostatically induced exposure surface on a cap dolostone in the NE of the West African craton, but this appears to be a singular occurrence of phosphorite formed during a Neoproterozoic deglaciation.

The association of chemical sediments with Neoproterozoic glacial deposits has long been known. In fact, Neoproterozoic glaciation was discovered in a number of regions as a result of the search for economic Fe and Fe–Mn deposits (e.g. SW Brazil, NW Canada, Namibia). Glacial associated chemical sediments provide critical evidence concerning the nature of Neoproterozoic glaciations and their aftermaths, in the form of geochemical records of the waters from which they were precipitated, and indirectly the atmosphere with which those waters interacted.

Here, we briefly review the distribution, lithological association, sedimentology and palaeoenvironmental significance of orthochemical sediments deposited during Neoproterozoic glaciations and deglaciations. They include sedimentary Fe and Fe–Mn deposits and cap-carbonate sequences, of which 'cap dolostones' *sensu stricto* form the basal transgressive systems tracts. Barite ($BaSO_4$) and phosphorite mineralization occurs locally within Marinoan cap dolostones. More information on geologic setting, stratigraphic relations, geochemistry and isotopic characteristics is given in the appropriate regional chapters. Palaeogeographies of the deposits (Fig. 5.1) are based on global model maps for 715 Ma (Sturtian) and 635 Ma (Marinoan), created by the Tectonics Special Research Centre in Perth, Western Australia (Li *et al.* 2008; Hoffman & Li 2009). The maps were constructed on the basis of palaeomagnetic constraints, the mantle plume record and palaeocontinental tectonic genealogy, factors that are largely independent of palaeoclimate. The Sturtian glaciation persisted until 659 ± 6 Ma in its type area (Fanning & Link 2008), by which time the model palaeogeography (Li *et al.* 2008) was intermediate between 715 and 635 Ma (Fig. 5.1).

Fe and Fe–Mn deposits

Distribution in time and space

The palaeogeographic distribution of synglacial Fe and Fe–Mn sedimentary deposits is shown in Figure 5.1 (Table 5.1). The economic Fe–Mn ores of the Jacadigo Group in the Urucum District of southwestern Brazil and eastern Bolivia (see below) were tentatively assigned to the terminal Cryogenian (Marinoan) glaciation (Hoffman & Li 2009) through correlation with the Puga diamictite in the adjacent Paraguay fold belt (Alvarenga & Trompette 1992; Trompette 1994; Trompette *et al.* 1998). The Puga diamictite is capped by a diagnostic Marinoan-type cap-carbonate sequence (Nogueira *et al.* 2003, 2007; Trindade *et al.* 2003; Font *et al.* 2005, 2006; Alvarenga *et al.* 2008). However, no cap carbonate is preserved in the Jacadigo Group, which occupies a transverse rift-basin on the cratonic foreland of the Paraguay fold belt (Trompette *et al.* 1998). The true age of the Jacadigo Group, Sturtian or Marinoan, is unknown. Similarly, Fe formation in the glaciogenic Rizu Formation of central Iran was tentatively assigned to the Marinoan glaciation (Hoffman & Li 2009) on the basis of a reported cap dolostone (Kianian & Khakzad 2008), but details are lacking. The reassignment of the Jacadigo and Rizu Fe formations to the Sturtian glaciation (Fig. 5.1) is therefore permissible, but arbitrary. In either palaeogeographic reconstruction (Fig. 5.1), the Fe- and Fe–Mn deposits formed disproportionately within 30° of the palaeoequator, and at the margins of ocean basins that were both internal (Jiangkou, Sturt, Rapitan, Surprise, Numees and Chuos) and external (Rizu, Tany) to the fragmented Rodinia supercontinent.

From: ARNAUD, E., HALVERSON, G. P. & SHIELDS-ZHOU, G. (eds) *The Geological Record of Neoproterozoic Glaciations*. Geological Society, London, Memoirs, **36**, 67–80. 0435-4052/11/$15.00 © The Geological Society of London 2011. DOI: 10.1144/M36.5

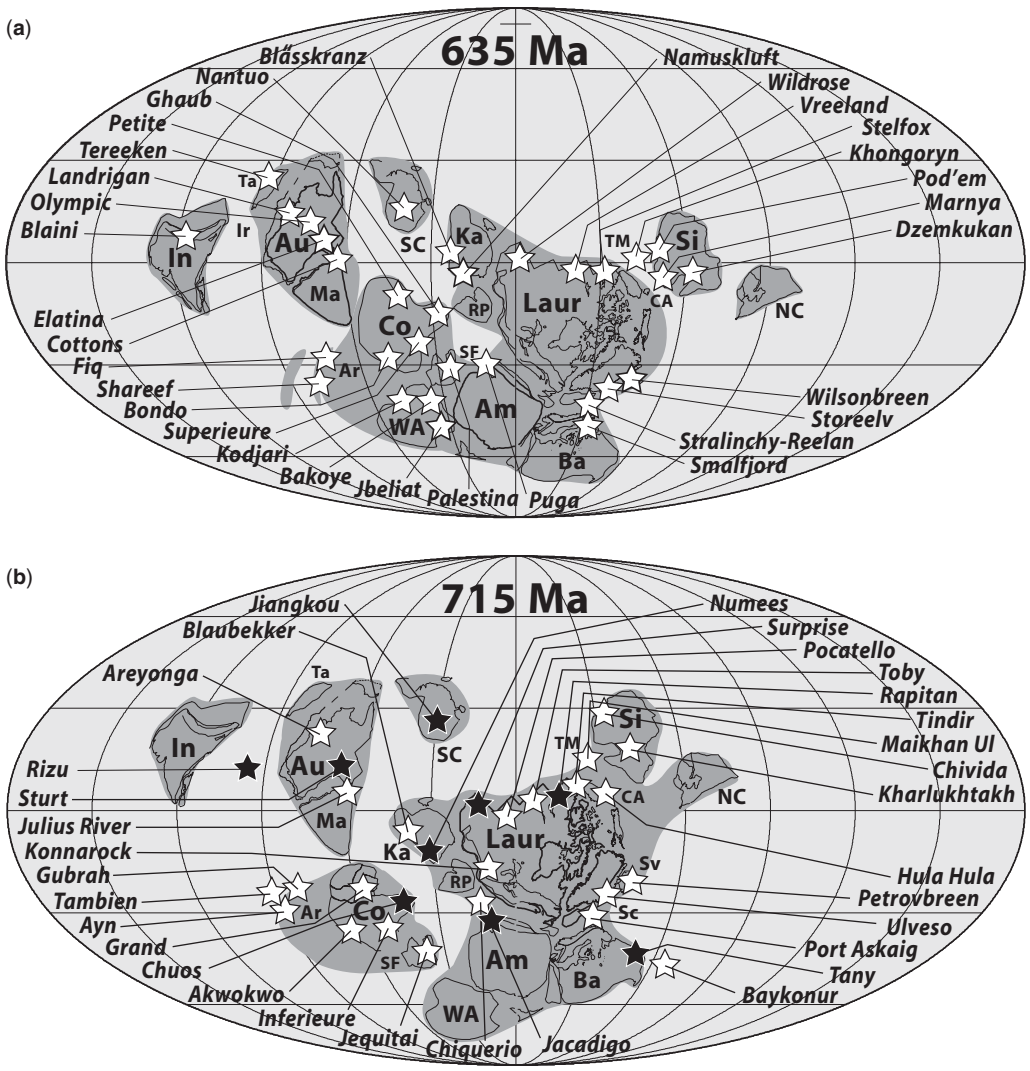

Fig. 5.1. Palaeogeographic maps for 715 Ma and 635 Ma (Hoffman & Li 2009) showing distribution of (**a**) Sturtian and (**b**) Marinoan glaciogenic deposits (open stars), and synglacial Fe or Fe–Mn deposits (black stars). Palaeocontinents: Ar, Arabia; Am, Amazonia; Au, Australia; Ba, Baltica; CA, Chukotka–Arctic Alaska; Co, Congo; In, India; Ir; central Iran; Ka, Kalahari; Laur, Laurentia (including Sc, Scotland and Sv, Svalbard); Ma, Mawson; NC, North China; SF; São Francisco; RP, Rio de la Plata; SC, South China; Si, Siberia; Ta, Tarim; TM, Tuva-Mongolia; WA, West Africa. Palaeocontinents constrained by penecontemporaneous palaeomagnetic data have heavy lines. The Sturtian glaciation persisted to *c.* 660 Ma in some areas (South Australia and western USA), by which time the model palaeogeography was intermediate between 715 and 635 Ma. Assignment of Fe formations in the Jacadigo Group (Am) and Rizu Formation (Ir) to the Sturtian glaciation is uncertain. Correlation of Fe formation in the Gariep Belt (Ka) with the glaciogenic Numees Formation follows Macdonald *et al.* (2011).

Lithological associations

Impure to pure haematite–jaspilite occurs within intervals of parallel-laminated argillite, ferruginous argillite and Mn-oxides. Those identified in Figure 5.1 host outsize clasts (lonestones) of intrabasinal and extrabasinal (crystalline basement) derivation, generally interpreted as ice-rafted debris. Many occur in contact with massive to poorly stratified diamictite, inferred to be peri- or subglacial in origin based on the presence of faceted, striated and/or preferentially oriented clasts. Sizeable Fe and Fe–Mn deposits occur in intervals that are sandwiched between composite diamictite horizons, locally of great thickness (e.g. Braemar, Holowilena, Jakkalsberg, Sayunei, Tany). Smaller deposits are intimately interfingered with diamictite (e.g. Braemar, Chuos). Still other deposits lack diamictite but the presence of dropstones of intra- and extrabasinal origin suggest a

Table 5.1. *Cryogenian glacigenic Fe and Fe–Mn deposits*

Palaeocontinent	Location	Host strata	References
Amazonia	Urucum	Jacadigo	Dorr (1945), Urban *et al.* (1992), Klein & Ladeira (2004)
Australia	Braemar	Yudnamutana	Whitten (1970), Lottermoser & Ashley (2000)
Baltica	Middle Urals	Vil'va	Chumakov (1992, 2007)
Congo	Damara Belt	Chuos	Martin (1965*a*), Badenhorst (1988), Clifford (2008)
Kalahari	Gariep Belt	Numees	Macdonald *et al.* (2011)
Laurentia	NWT-Yukon	Rapitan	Young (1976), Yeo (1981, 1986), Klein & Beukes (1993)
Laurentia*	Death Valley	Surprise	Corsetti & Kaufman (2003)
Lut (central Iran)	Kerman	Rizu	Kianian & Khakzad (2008)
South China	Yangtze platform	Jiangkou	Jiafu *et al.* (1987)
Tuva-Mongolia	Erzin	Maikhan Ul	Ilyin (2009)

*In the collisional model for Laramide orogeny (Hildebrand 2009), the Death Valley area as well as most other Cryogenian glacial formations in the western USA and British Columbia are considered to be exotic with respect to Laurentia before the Late Cretaceous.

subaqueous proglacial setting (e.g. Urucum). Parallel-laminated facies hosting haematite–jaspilite are commonly interpreted as interglacial or interstadial, but they might alternatively represent maximum glacial stages, when outlet glaciers were blocked by thick multi-annual sea ice (Dowdeswell *et al.* 2000).

Geochemical characteristics

Compared with Archaean–Palaeoproterozoic banded Fe formations, Cryogenian Fe deposits are mineralogically simple, consisting of haematite, chert (jasper) and minor carbonate. Fe contents range up to 50% Fe_2O_3. Organic contents are negligible and carbonates are moderately depleted in ^{13}C, suggesting that organic matter originally present was respired with Fe(III) serving as electron acceptor. Normalized rare earth element profiles are distinct from Archaean–Palaeoproterozoic Fe formations, being more strongly depleted in light rare earth elements, and having much weaker positive Eu anomalies or none at all (Klein & Beukes 1993; Graf *et al.* 1994; Klein & Ladeira 2004; Klein 2005). The Cryogenian profiles are more similar to those of modern seawater, and hydrothermal contributions are more diluted than in more ancient Fe formations.

Notable examples

Jacadigo Group, Urucum District, Mato Grosso do Sul, Brazil. Economic Fe–Mn oxide ores of the Jacadigo Group occur in stratigraphically isolated fault blocks in the Urucum District of southwestern Brazil and adjacent Bolivia (Dorr 1945; Walde *et al.* 1981; Urban *et al.* 1992; Trompette *et al.* 1998). A lower Urucum Formation, comprising conglomerate, sandstone and black shale, is overlain by the Santa Cruz Formation, a sequence of Mn ore horizons, chiefly composed of cryptomelane ($K_2Mn_8O_{16}$), interspersed with ferruginous sandstone and up to 270 m of haematite–jaspilite. All units of the Santa Cruz Formation carry dropstones of basement and subordinate carbonate lithologies. They are interpreted to be ice-rafted and the Jacadigo Group to have been deposited in a partly ice-covered fjord-like basin (Urban *et al.* 1992). The alternation of Mn and Fe ores is attributed to cycles of glacial advance and retreat. Enhanced fluxes of oxygenated subglacial meltwater during glacial retreats favoured Mn precipitation in ice-covered anoxic parts of the basin. Reduced fluxes of subglacial meltwater during glacial advances favoured Fe deposition (Urban *et al.* 1992). The Jacadigo Group lies in the cratonic foreland of southern Amazonia, close to the Paraguay fold belt of Early Cambrian (Brasiliano) age within which glaciogenic diamictite of the Puga Formation (Alvarenga & Trompette 1992) is sharply overlain by a typical Marinoan-type cap dolostone (Nogueira *et al.* 2003, 2007; Trindade *et al.* 2003; Font *et al.* 2005, 2006; Alvarenga *et al.* 2008). No cap carbonate is preserved on the Jacadigo Group, however, so the correlation of the Jacadigo and Puga groups is uncertain, as is, therefore, the age of the Urucum Fe–Mn deposits.

Rapitan Group, northern Canadian Cordillera. Haematite–jaspilite and ferruginous argillite occur within glaciogenic diamictite of the Rapitan Group and correlatives discontinuously for *c.* 800 km along the strike of the Ogilvie and Mackenzie mountains (Young 1976; Yeo 1981, 1986; Eisbacher 1985; Klein & Beukes 1993; Macdonald *et al.* 2011; Hoffman & Halverson 2011; Macdonald & Cohen 2011). The glacial onset coincided with a major flood basalt episode across Arctic Laurentia, bimodal representatives of which underlie and intercalate the basal Rapitan diamictite in the Ogilvie Mountains, constraining its age at 717 Ma (Macdonald *et al.* 2010). Haematite–jaspilite is up to 120 m thick in an ice-proximal section (Iron Creek, NW Mackenzie Mtns), where it is sandwiched between composite diamictite complexes hundreds of metres thick. Jaspilite first appears as 2-m-thick septa between individual diamictite bodies in the upper part of the lower complex (Mount Berg Formation). In a more distal section (Hayhook Lake, SE Mackenzie Mountains), 14 m of ferruginous argillite and haematite–jaspilite conformably overlie 650 m of maroon-coloured siltstones with graded sandy beds and a sprinkling of small dropstones, some of which were redeposited as debrites. The jaspilite itself contains rounded boulders of quartz-monzonite and is overlain disconformably by the upper diamictite complex (Shezal Formation). The basal part of the otherwise olive-coloured Shezal diamictite acquired its maroon colour and numerous jaspilite clasts from the underlying Sayunei Formation. Fe-isotope and Ce anomaly profiles suggest that the haematite–jaspilite records subsidence of the basin floor across a redoxcline in the water column (Klein & Beukes 1993; Hoffman & Halverson 2011).

Jakkalsberg Member (Numees Formation, Port Nolloth Group), Gariep Belt, Namibia and South Africa. Haematite- and magnetite–jaspilite with basement-derived lonestones make up the Jakkalsberg Member of the Numees Formation in thrust sheets intersected by the Orange River (Frimmel & von Veh 2003). The Numees Formation has long been assumed to be the younger of two glaciogenic horizons in the Gariep Belt, the older being the Kaigas Formation (Frimmel 2008, 2011). Recently, a mid-Ediacaran age for the Numees glaciation has been advocated from carbonate Pb/Pb dating (Fölling *et al.* 2000), $^{87}Sr/^{86}Sr$ ratios of 0.7082–0.7085 (Fölling & Frimmel 2002), correlations with dated South American strata (Frimmel 2004, 2008) and micropalaeontological findings (Gaucher *et al.* 2005). The microfossils do not appear to be diagnostic, however, and the Sr isotope ratios (0.001 higher than typical Marinoan values; Halverson *et al.* 2007) are potentially attributable to diagenesis, as are the Pb/Pb dates. Subsequent remapping of the least-deformed and least-allochthonous sections prompted a reassessment of stratigraphic correlations between the autochthon and thrust sheets within the belt (Macdonald *et al.* 2011). The younger autochthonous diamictite, previously correlated with the Numees Formation, is now proposed as an independent glaciogenic horizon, the Namuskluft diamictite (Macdonald *et al.* 2011). It is capped by a pale dolostone (Dreigratberg Member, previously conflated with the Bloeddrif Member, of the Holgat Formation) containing hallmark features of Marinoan cap dolostones–sheet-crack cements, tubestone stromatolites and giant wave ripples (Hoffman & Macdonald 2010). In contrast, the jaspilite-bearing Numees diamictite is overlain by a dark microbial limestone with roll-up structures, characteristic of Sturtian cap carbonates (see below). Accordingly, the Jakkalsberg jaspilite is probably older Cryogenian (Sturtian) in age, and the Kaigas Formation may represent a pre-Sturtian (*c.* 0.74 Ga) diamictite of uncertain origin (Macdonald *et al.* 2011).

Central Flinders Ranges (Holowilena) and Nackara arc (Braemar), South Australia. Like the more ice-proximal (Iron Creek) section in NW Canada, haematite–jaspilite and associated ferruginous argillite in South Australia are sandwiched between a conformably underlying diamictite complex (Pualco 'Tillite') and a disconformably overlying complex (Wilyerpa Formation) dominated by diamictite (Whitten 1970; Preiss 1987; Lottermoser & Ashley 2000). In the Flinders Ranges, ferruginous argillite hosts sporadic lenses of boulders, some of which are grooved and striated, ferruginous diamictite, and rare lenses of haematite–jaspilite with rafted dropstones. In the more basinward Nackara arc, haematite–jaspilite is interrupted by thin units of ferruginous diamictite. Sorted sandstones occur within the diamictite complexes in both areas. Correlation of the Holowilena and Braemar jaspilites is uncertain, but they and the bounding Pualco and Wilyerpa diamictites are referred to the Sturtian glaciation (Preiss 1987).

Cap-carbonate sequences

The continuous layers of carbonate that blanket Cryogenian glaciogenic sequences or their equivalent disconformities are called 'cap' carbonates. Clearly associated with syndeglacial flooding (Kennedy 1996; Bertrand-Sarfati *et al.* 1997; Hoffman *et al.* 2007), they occur on virtually every palaeocontinent and even in siliciclastic-dominated successions (Table 5.2). Lithologically and isotopically, Sturtian and Marinoan cap carbonates are distinct, both from each other (Kennedy *et al.* 1998; Halverson & Shields 2011) and from most other Neoproterozoic carbonates (Hoffman 2011). Hoffman & Schrag (2002) proposed that depositional sequences related to Neoproterozoic syndeglacial flooding be called 'cap-carbonate sequences'. 'Cap dolostones', *sensu stricto*, are the transgressive tracts of cap-carbonate sequences and feature a suite of idiosyncratic sedimentary features (e.g. size-graded peloids, sheet-crack cements, tubestone stromatolites, giant wave ripples, primary and early diagenetic barite). Transgressive cap dolostones have rarely been documented in Sturtian cap-carbonate sequences and are thin ($<$1.0 m) where present (Smith *et al.* 1994). Cap-carbonate sequences have aroused intense interest because they are unique to Proterozoic glaciations and record physical, chemical and biological conditions during and immediately after global deglaciation (Aitken 1991; Grotzinger & Knoll 1995; Kennedy, 1996; Hoffman *et al.* 1998, 2007; James *et al.* 2001; Kennedy *et al.* 2001; Higgins & Schrag 2003; Ridgwell *et al.* 2003; Trindade *et al.* 2003; Shields 2005; Allen & Hoffman 2005; Font *et al.* 2005, 2006; Hurtgen *et al.* 2006; Jiang *et al.* 2006; Bao *et al.* 2008; Le Hir *et al.* 2009; Hoffman 2011).

Marinoan-type (basal Ediacaran) cap-carbonate sequences

The extent and uniqueness of Marinoan cap dolostones was first appreciated in Australia (Dunn *et al.* 1971; Rankama 1973) and the presence of barite in cap dolostones was first recognized in West Africa (Deynoux & Trompette 1976). The smooth and abrupt, yet conformable, contact between glaciogenic and related detritus and cap dolostones is so distinctive and widespread that it was selected as the basis of the Global Stratotype Section and Point (GSSP) for the Ediacaran Period (Knoll *et al.* 2006), the first Period boundary to be defined strictly on lithologic grounds. A tuff at the top of the presumed correlative cap dolostone in South China yields a $^{238}U-^{206}Pb$ (IDTIMS) zircon date of 635.2 $\pm$ 0.4 Ma (Condon *et al.* 2005). A statistically indistinguishable $^{238}U-^{206}Pb$ (SHRIMP) zircon date of 636.3 $\pm$ 4.9 Ma was obtained from a tuff near the base of the underlying Nantuo glaciogenic diamictite (Zhang *et al.* 2008). The presumed

Table 5.2. *Average thickness and idiosyncratic features of Marinoan cap dolostones in numerical order of abundance*

Palaeocontinent	Glaciation	Cap dolostone (ref.)	Metres	LAC	PEL	GWR	SCC	TBS	TPB	DGB	SFB
Amazonia	Puga	Mirassol d'Oeste (1)†	24	√	√	√	–	√	–	–	–
Arabia	Gadir Manqil (Fiq)	Hadash (2)	4.5	–	–	–	–	–	–	–	–
Arctic Alaska	No deposits	Nularvik (3)†	35	√	√	√	–	√	–	–	–
Australia	Olympic	Mount Doreen (4)	4	√	√	√	√	–	–	–	√
Australia	Elatina	Nuccaleena (5)	5	–	–	√	√	–	–	–	–
Australia	Cottons	Cumberland Creek (6)	6	√	√	√	–	–	–	–	–
Australia	Landrigan	Lower Stein (7)	8.5	√	–	√	–	–	–	–	–
Baltica	Smalfjord	Lower Nyborg (8)	5	–	–	–	√	–	–	–	√
Congo	Ghaub	Keilberg (9)†	38	√	√	√	√	√	–	–	–
Congo	Petit Conglomérat	Calcaire rosé (10)	10								
Congo	Upper Tilloid	C1 Dolomie rosé (11)	10								
India	Blaini	Upper Blaini (12)	10								
Kalahari	Namuskluft	Dreigratberg (13)	25	√	√	√	√	√	–	–	–
Kalahari	Blässkranz	Tsabesis (14)	21	√	–	–	–	–	–	–	–
Kalahari	No deposits	Bildah (15)†	80	√	–	–	√	√	–	–	–
Laurentia	Stelfox (Ice Brook)	Ravensthroat (16)†	12	√	√	√	–	√	–	–	√
Laurentia	Storeelv	Lower Canyon (17)	10	√	–	–	–	–	–	–	–
Laurentia	Wilsonbreen	Lower Dracoisen (18)	10	√	√	√	–	–	–	–	–
Laurentia	Stralinchy-Reelan	Cranford (19)	4	√	–	–	√	–	√	–	–
Laurentia	Upper Tindir	Hard Luck (20)	4	–	–	–	√	–	–	–	–
Laurentia*	Wildrose	Noonday (21)	175	√	√	√	–	√	–	–	–
Siberia	Ulyakha	Lower Ozerki (22)	35	√	–	–	–	–	–	–	–
South China	Nantuo	Lower Doushantuo (23)	4	–	√	–	√	–	√	√	–
Tarim	Tereeken	Lower Zhamoketi (24)	6	–	√	–	–	–	–	–	–
Tuva-Mongolia	Khongoryn	Ol (25)†	15	√	√	√	√	√	–	√	√
Tuva-Mongolia	Khesen	Baxha (26)	4	–	–	–	√	–	–	–	√
West Africa	Fersiga	Oued Djouf (27)	6	–	–	–	√	–	√	–	–
West Africa	Jbéliat	Amogjar (28)	5	–	√	–	–	–	√	√	–
West Africa	Banboli	Mid Sud-Banboli (29)	1.5	√	√	–	√	–	√	√	–

*In the collisional model for Laramide orogeny (Hildebrand 2009), Wildrose-Noonday strata and most other Cryogenian glacial formations in the western USA and British Columbia are considered to be exotic with respect to Laurentia before the Late Cretaceous.

†Former-aragonite seafloor cement above cap dolostone. LAC, low-angle cross-laminae; PEL, peloids; GWR, giant wave ripples; SCC, sheet-crack cements; TBS, tubestone stromatolite; TPB, tepee breccia; DGB, diagenetic barite; SFB, seafloor barite.

References: (1) Nogueira *et al.* (2003); (2) Allen *et al.* (2004); (3) Macdonald *et al.* (2009); (4) Kennedy (1996); (5) Plummer (1978); (6) Calver & Walter (2000); (7) Corkoron (2007); (8) Edwards (1984); (9) Hoffman *et al.* (2007); (10) Cahen & Lepersonne (1981); (11) Cahen (1950); (12) Kaufman *et al.* (2006); (13) Hoffman & Macdonald (2010); (14) PFH observations; (15) Hegenberger (1993); Prave *et al.* (2011); (16) James *et al.* (2001); (17) Hambrey & Spencer (1987); (18) Halverson *et al.* (2004); (19) McCay *et al.* (2006); (20) Macdonald & Cohen (2011); (21) Corsetti & Grotzinger (2005); (22) Sovetov & Komlev (2005); (23) Jiang *et al.* (2006); (24) Xiao *et al.* (2004); (25) Macdonald (2011); (26) Macdonald & Jones (2011); (27) Bertrand-Sarfati *et al.* (1997); (28) Shields *et al.* (2007); (29) Nédélec *et al.* (2007).

correlative Ghaub diamictite in Namibia has an indistinguishable $^{238}U-^{206}Pb$ (IDTIMS) zircon date of 635.6 $\pm$ 0.5 Ma (Hoffmann *et al.* 2004). Marinoan cap dolostones are therefore assumed to have been deposited at 635 Ma.

Distribution and thickness. The median and average thicknesses of 29 Marinoan cap dolostones on 15 palaeocontinents (Table 5.2) are 9 m and 18 m, respectively (Hoffman *et al.* 2007). As there are large facies-controlled variations in thickness in some areas, these estimates are based on area-weighted average thicknesses, where data permit. On the Otavi platform (Congo palaeocontinent) of Namibia, for example, the Keilberg cap dolostone is 6–10 m thick on the distal foreslope, up to 100 m on the upper foreslope, up to 75 m on the raised outer platform, and 20–25 m on the deepened inner platform (Fig. 5.2). In general, cap dolostones are thickest on palaeotopographic highs and thinnest in lows, converse to underlying glacial deposits. Observed inner-shelf deepening is characteristic of glaciated margins (Anderson 1999). If cap dolostones averaged 18 m in thickness over 20% of the present continental surface area (including shelves), they would contain *c.* 2.6×10^5 Pg (Gt) of C. This dwarfs the 3.8×10^4 Pg of dissolved inorganic C in the present ocean. According to the palaeogeography in Figure 5.1a, the maximum thickness of cap dolostones increased from 5 m above 40° palaeolatitude, to 10 m above 30°, 25 m above 20°, 38 m above 10° and 175 m at the palaeoequator (Hoffman & Li 2009).

Expanded and condensed sequences. The decompacted thickness of a cap-carbonate sequence (as distinct from a cap dolostone), minus the effect of sediment loading, is a measure of the accommodation created before and during its deposition. The lowering and raising of global mean sea level attending the growth and decay of ice sheets creates no permanent accommodation if global ice-sheet volume was the same before and after a glaciation. Permanent accommodation (i.e. outlasting isostatic adjustments) was created during Cryogenian glaciations by net erosion, compaction and tectonic subsidence. Glacial palaeofjords, for example, contain expanded cap-carbonate sequences compared with adjacent uplands (Fig. 5.3). Similarly, areas undergoing rapid tectonic subsidence like the Otavi platform, on which the Sturtian and Marinoan cap-carbonate sequences are each 250–400 m thick, contrast with areas like the Taoudeni Basin of the West African craton (Deynoux 1985; Shields *et al.* 2007), where subsidence rates were low and cap-carbonate sequences are highly condensed, outside of incised palaeovalleys (Fig. 5.3). Condensation may also occur in fully marine settings where sedimentation rates were inadequate to fill the existing accommodation space. On the distal foreslope of the Otavi platform, for example, drowning at the terminal deglaciations was effectively permanent (Halverson *et al.* 2005). The cause of condensation of the lower Doushantuo Formation cap-carbonate sequence of South China (low sedimentation rate or lack of accommodation?) depends on whether tepee-like breccias and associated early diagenetic barite mineralization in the cap dolostone are submarine (Jiang *et al.* 2006) or subaerial (Zhou *et al.* 2010) in origin, respectively.

Transgressive cap dolostones in expanded sequences. Cap dolostones are typically pale pinkish (yellowish-grey weathering) dolomicrites, with palimpsest micro- to macro-peloidal textures indicating deposition as silt and sand- and granule-sized aggregates. Those in expanded sequences lack the diagenetic overprint experienced by those in condensed sequences, which we treat separately. The former (e.g. Cumberland Creek, lower Canyon, lower Dracoisen, Dreigratberg, Keilberg, Mirassol d'Oeste, Mount Doreen, Nuccaleena, Ol, lower Pertatataka, Ravensthroat, Sentinel Peak, lower Stein, Tsabesis, and lower Zhamoketi; see Table 5.2) are invariably laminated, with each lamina representing a sedimentation unit composed of well-sorted, graded or reverse-graded peloids, up to 3 mm in diameter, terminating with a micropeloidal drape (Aitken 1991; Kennedy 1996; Calver & Walter 2000; James

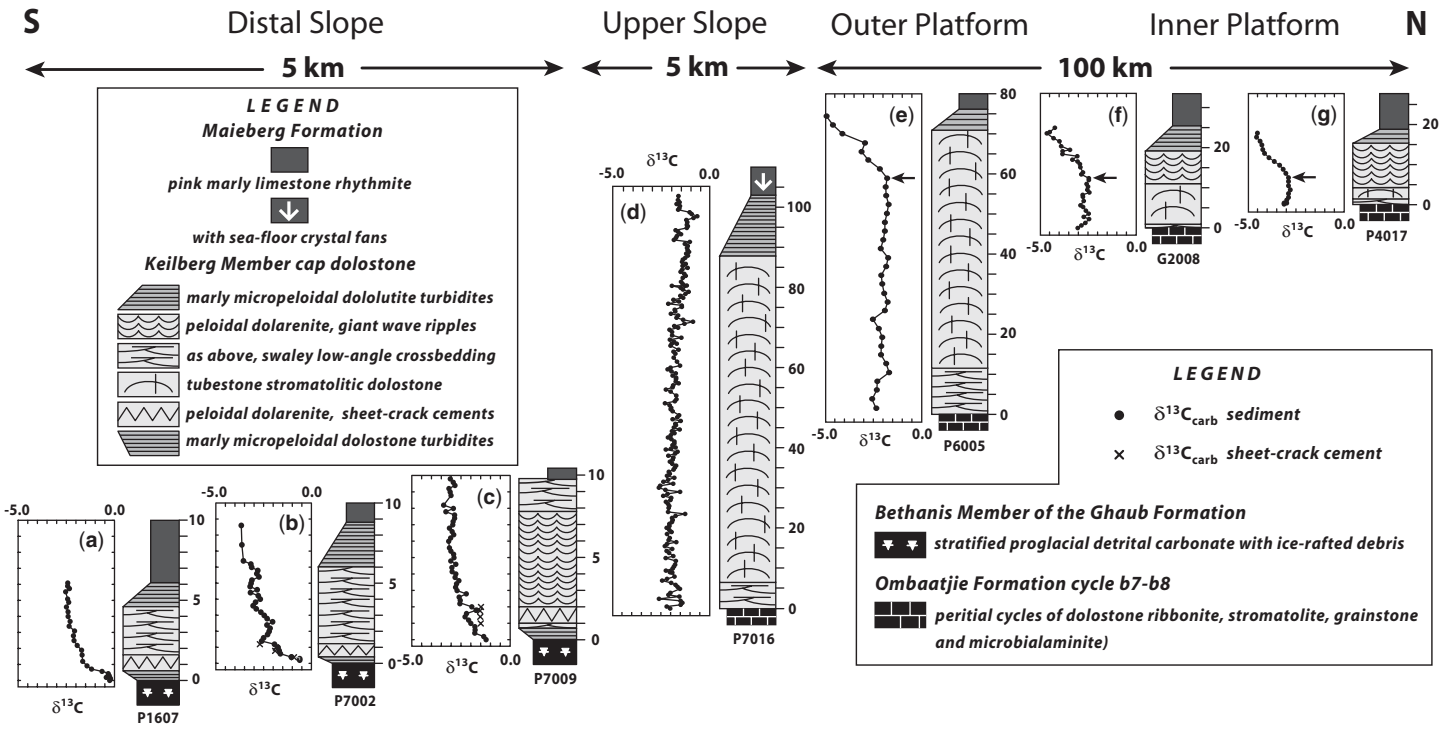

Fig. 5.2. Representative lithologic columns and $\delta^{13}C$ profiles of the Keilberg cap dolostone (Marinoan) in contiguous palaeobathymetric zones of the Otavi platform, northern Namibia (Hoffman *et al.* 2007). The datum for platform columns (**e**–**g**) is the inflection point (arrows) in isotopic profiles. Each column records part of an overall sigmoidal profile, implying diachronous deposition during progressive marine inundation. The systematic nature of profiles rules out a detrital origin for dolomite and a diagenetic origin for $\delta^{13}C$ values. Note that values for isopachous dolomite sheet-crack cement (crosses) in (**b**) and (**c**) are indistinguishable from host dolopelmicrite (dots).

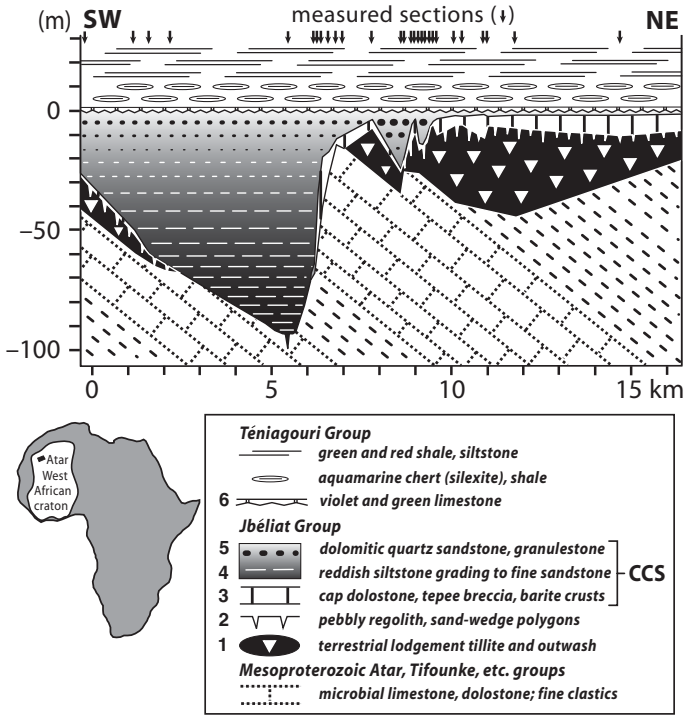

Fig. 5.3. Stratigraphic cross-section of the glaciogenic Jbéliat Group (Marinoan?) based on sections measured along Atar Cliff, Mauritania, by present authors PFH and GPH and Adam C. Maloof (Hoffman & Schrag 2002). The cap-carbonate sequence (CCS) includes cap dolostone (unit 3) and regressive highstand deposits (units 4 and 5) preserved only in palaeovalleys. The datum is the top of the cap-carbonate sequence. Silicified shale (silexite) belongs to the succeeding Téniagouri depositional sequence and need not be genetically related to glaciation.

et al. 2001; Halverson *et al.* 2004; Xiao *et al.* 2004; Font *et al.* 2006; Nédélec *et al.* 2007). Locally, cap dolostones begin with a coarsening-upward interval of discrete, parallel-sided, normally graded, sedimentation units interpreted as turbidites, separated by argillaceous partings (Lithofacies I of Kennedy 1996; Hoffman & Macdonald 2010). The turbidites, where present, grade upward into laminated but less discretely bedded dolostone with ubiquitous low-angle crossbedding, including toplaps, onlaps and downlaps (Lithofacies II of Kennedy 1996). Kennedy (1996) attributes the low-angle crossbedding to asymmetric synsedimentary dissolution and/or semi-plastic slumping of originally parallel-sided strata deposited below the storm wave base. A simpler and more conventional interpretation is that low-angle crossbedding records wave action above the storm wave base. This interpretation is consistent with the sorted macropeloids and implies initial shoaling subsequent to the underlying turbidites (Hoffman & Macdonald 2010). Intertidal–supratidal indicators (e.g. fenestral texture or other desiccation features, abraded intraclasts, beach 'rosettes', channels and levees, polygonal tepees and related breccias) are absent (Kennedy 1996). The low-angle cross-bedded lithofacies is dominant and within it occurs a triad of highly idiosyncratic structures in a broadly consistent vertical sequence, although all three are rarely present in a single section (Fig. 5.2). The structures are described in more detail in Hoffman (2011, and references therein) and are, in order of appearance:

- sheet-crack cements (Kennedy 1996; Corkeron 2007; Hoffman & Macdonald 2010) – bedding-parallel, variably buckled, fibrous isopachous, void-filling dolospar, confined to a continuous metre-thick zone of variable intensity near the base of the cap dolostone in distal slope sections, typically just above basal turbidites;
- tubestone (geoplumb) stromatolites (Cloud *et al.* 1974; Hegenberger 1993; Corsetti & Grotzinger 2005) – metre- to decametre-scale mounds within which arched microbial growth laminae are interrupted by tube-like structures, invariably oriented palaeovertically, defined by parallel-laminated dolomicrite with meniscus-like curvature, variably replaced by late-stage void-filling cement;
- giant wave ripples (Allen & Hoffman 2005; Hoffman & Li 2009) – trochoidal megaripples with high aspect ratios, aggradational development, and crestward-coarsening bidirectional laminae that interdigitate in the crestal region.

Interpretations of these structures differ. Kennedy *et al.* (2001) relate sheet-crack cements to permafrost clathrate destabilization by marine flooding, but $\delta^{13}C$ values of the isopachous dolospar cement are not extraordinarily depleted (Fig. 5.2), nor is $\delta^{34}S$ of cap dolostone enriched as predicted (Shields 2005). Corkeron (2007) attributes sheet-crack cements to pore-fluid overpressure associated with differential shale-carbonate compaction. Hoffman & Macdonald (2010) suggest that pore-fluid overpressures signal rapid falls in regional sea level associated with the disappearance of ice sheets and the loss of their gravitational 'pull' on adjacent ocean waters. Cloud *et al.* (1974) interpret the tubular structure in stromatolites as fluid- or gas-escape channels on account of their geoplumb orientation. Corsetti & Grotzinger (2005) interpret them as microbial growth structures. Hoffman (2011) attempts to estimate the inclination of the upper foreslope of the Otavi platform from the mean dip of stromatolitic layering after restoring the contained tubes to vertical. Giant wave ripples were first interpreted as supratidal tepee structures (Eisbacher 1985), but their crestlines are straight and parallel, not polygonal like true tepees, and they lack the breccias and void-filling cements diagnostic of supratidal tepees (Kendall & Warren 1987). Gammon *et al.* (2005) describe a tepee-like structure in the Nuccaleena cap dolostone and relate it to a growth fault, but giant wave ripples in the same formation lack faults and the one described by Gammon *et al.* (2005), which is oriented perpendicular to bedding, could not have had a slip vector that was parallel or subparallel to the outcrop surface (i.e. the plane of their two-dimensional kinematic analysis), compromising the growth fault interpretation. Allen & Hoffman (2005) interpret them as unusually large, steep and aggradational wave ripples, related to the action of long-period waves in the lower part of the ocean mixed layer, driven by strong sustained winds (not hurricanes). Hoffman & Li (2009) find that crestal orientations globally had meridional (north–south) mean orientations and that zonal (east–west) orientations were absent, consistent with zonal and not with cyclonic winds.

Sorted peloids, low-angle crossbedding, stromatolites and giant wave ripples signify that cap dolostones were deposited above the storm wave base and at least partly in the euphotic zone. The occurrence of shallow-water structures over a large range of palaeodepths implies diachronous deposition attending a large rise in sea level, consistent with the fragmented $\delta^{13}C$ records of cap dolostones from different palaeodepths (Fig. 5.3). The estimated magnitude of the rise of more than a kilometre implicates global ice-sheet melting (so-called 'glacioeustasy') and links the timescales of deglaciation and cap-dolostone sedimentation (Kennedy 1996; Bertrand-Sarfati *et al.* 1997; James *et al.* 2001; Hoffman *et al.* 2007). Cap dolostones are locally postglacial, but globally syndeglacial.

Seafloor carbonate cement. In expanded sequences, cap dolostones are overlain conformably by deeper water limestone, limestone with dolostone turbidites, marlstone or shale. Seafloor cement, in the form of crystal fans of pseudomorphosed prismatic aragonite, built masses up to 100 m thick, localized by sea-bottom topography (Hoffman 2011). In magnitude, they dwarf other Neoproterozoic seafloor cements and differ from volumetrically comparable

Archaean–Palaeoproterozoic examples in having formed in the presence of micritic sedimentation (Sumner 2002).

Highstand deposits of cap-carbonate sequences. Regressive highstand deposits in expanded cap-carbonate sequences may be carbonate or clastic-dominated. The former begin with limestone rhythmite and shoal to dolostone grainstone beneath a well-developed subaerial sequence boundary. Grain-sized equivalent terrigenous deposits (shales, siltstones and sandstones) conformably overlie cap dolostones in many areas (e.g. in the Brachina Formation and the ABC Range Quartzite in South Australia). In the cratonic Taoudeni Basin of West Africa, highstand deposits are found in palaeovalleys but are missing on palaeotopographic highs (Fig. 5.3). This has led to misinterpretation. Silicified shale (silexite) of the Téniagouri Group (Fig. 5.3) and correlatives rest directly on the altered surface of the cap dolostone over vast areas of the craton, leading to the concept of a 'triad': tillite–carbonate–silexite. We concur with Bertrand-Sarfati *et al.* (1997), in that this concept should be abandoned. Deposition of the Téniagouri Group (and correlative Azlaf Group, Deynoux *et al.* 2006) cannot be related to the glacio-eustatic transgression and could be much younger (Bertrand-Sarfati *et al.* 1997).

Transgressive cap dolostones in condensed sequences. Where accommodation was lacking, cap dolostones aggraded or prograded to the supratidal zone, where they were subjected to intense meteoric and vadose diagenesis (Fig. 5.3). In such cases, primary marine dolopelmicrite was repeatedly fractured and re-cemented in tepee structures and related breccias (Kendall & Warren 1987). Barite is a major void-filling cement in tepee brecciated cap dolostone on the Yangtze platform of South China (Jiang *et al.* 2006) and the West African craton (Shields *et al.* 2007). Where cap dolostones were subaerially exposed (Fig. 5.3), highstand deposits are typically absent.

Sturtian-type (Cryogenian) cap-carbonate sequences

The contacts between Sturtian glaciogenic deposits and cap carbonates, like Marinoan ones, are characteristically singular, smooth, abrupt and conformable. Sturtian cap carbonates are lithologically distinct: where Marinoan cap dolostones are pale in colour (<0.1 wt% total organic carbon, TOC), arenaceous in texture and display wave-generated structures. Sturtian cap-carbonate sequences typically begin with fetid, dark grey, parallel laminated, micritic limestone (rarely rhodochrosite, $MnCO_3$), with or without parallel-sided graded beds (turbidites) and debrites (Tojo *et al.* 2007). In Namibia, the Sturtian cap-carbonate sequence continues with up to 200 m of continuous sublittoral dolostone microbialaminite, featuring microbial rollup structures, neptunian dykes and inclined zones of high primary porosity overlain by humped microbialaminite (Pruss *et al.* 2010). The sublittoral microbialaminite extravaganza eventually grades up into cross-bedded grainstone, ending at a tepee brecciated sequence boundary.

Compared with Marinoan cap-carbonate sequences, where transgressive tracts (i.e. cap dolostones) are well developed, shallow-water transgressive tracts are thin (Smith *et al.* 1994) or absent in Sturtian cap-carbonate sequences. Typically, deepwater deposits directly overlie beveled supraglacial surfaces. The simplest explanation for the difference is a below-critical saturation state with respect to carbonate in the surface ocean during Sturtian deglaciation (Hoffman & Schrag 2002).

Mid-Ediacaran cap carbonate sequences

Most mid-Ediacaran glaciogenic horizons lack cap carbonates (e.g. Serra Azul, Squantum, Mortensnes, Moelv, Vil'chitsi, Loch ne Cille, Luoquan, Hankalchough and Croles Hill diamictites). Up to 40 cm of argillaceous limestone overlies glacial marine diamictite in two sections of the short-lived, 582 Ma Gaskiers Formation on the Avalon Peninsula of eastern Newfoundland, Canada (Myrow & Kaufman 1999). This cap carbonate is significant as the sole carbonate bed in the nearly 15-km-thick host succession. It lithologically and isotopically resembles the base of many Sturtian cap-carbonate sequences, although the amount of carbonate deposited overall is far smaller. Finally, the Egan diamictite represents a short-lived glacial incursion onto a mid-Ediacaran carbonate platform in the Kimberley region of Western Australia (Corkeron & George 2001). Diamictite and overlying conglomerate are overlain by *c.*15 m of dolostone with herringbone and trough crossbedding, and an additional *c.*15 m of interbedded quartz-arenite and silty dolostone with a distinctive stromatolite (*Tungussia julia*) horizon near the top. The carbonate sequence following the Egan glaciation resembles no other cap-carbonate sequence, including the one on the Landrigan diamictite in the same succession, stratigraphically well below the Egan, which has a recognizable Marinoan-type cap dolostone (Corkeron 2007).

Barite in Marinoan-type (basal Ediacaran) cap dolostones

Barite ($BaSO_4$) is a major constituent of certain Marinoan cap dolostones (Table 5.2). The mineral is easily recognizable in the field from its vitreous pearly lustre, bladed crystal habit and high specific gravity (4.3–5.0). Even where pseudomorphosed by calcite, its bladed crystals are distinct from aragonite, which is acicular (needlelike) in habit, forming pseudohexagonal prisms due to polysynthetic twinning. The palaeoenvironmental significance of barite rests with its highly redox-sensitive solubility in S-bearing aqueous solutions: the concentration of Ba in modern (oxic) seawater is only 1.4 ppb by atom, compared with 51 ppm in crustal rocks from which Ba in seawater is derived. Consequently, barite leached by anoxic pore waters from deep-sea carbonate ooze reprecipitates cumulatively at the sub-seafloor redox front as it migrates through the sediment column in response to sediment accumulation. However, it is doubtful that this process alone could provide a satisfactory explanation for either barite type in Marinoan cap dolostones, given their limited thickness.

Two types of barite in cap dolostones: primary and early diagenetic. Two types of barite have been described from Marinoan cap dolostones (Table 5.2): primary barite in the form of seafloor cement (Kennedy 1996; Hoffman & Halverson 2011) and early diagenetic barite associated with tepee and tepee-like breccias (Jiang *et al.* 2006; Shields *et al.* 2007). Seafloor barite forms at a laterally continuous horizon in the top few centimetres of cap dolostones. Tiny barite crystals self-assemble into macroscopic crystal fans or digitate aggregates. Interaction between barite growth and particulate sedimentation forms the basis for determining a seafloor origin, denoting precipitation of barite from the ambient water column. Early diagenetic barite forms void-filling isopachous crustose cements within breccias associated with tepee-like structures. The cause of tepee formation and brecciation is attributed to submarine methane venting (Jiang *et al.* 2006), or alternatively to evaporative pumping due to subaerial (supratidal) exposure in zones of marine–meteoric groundwater mixing (Shields *et al.* 2007). The second alternative is the conventional interpretation of tepee structures and associated breccias (Assereto & Kendall 1977; Kendall & Warren 1987).

Seafloor barite in central australia. In the Amadeus and Ngalia basins of central Australia, seafloor barite is associated with ferruginous domal stromatolite at the top of cap dolostones overlying Marinoan glaciogenic deposits of the Olympic and Mount Doreen formations, respectively (Kennedy 1996). Barite occurs

either as isolated bladed crystals (1–2 mm) or as large upward-oriented rosettes of bladed crystal (up to 4 cm high). The crystals 'grew at the sediment–water interface, as indicated by the upward-oriented growth habit, sediment drape defining crystal terminations, and presence of crystal fragments as detrital material within overlying sediment' (Kennedy 1996). In the Amadeus Basin, the barite-rich horizon is conformably overlain by reddish-grey laminated siltstone with limestone turbidites (Pertatataka Formation); in the Ngalia Basin it is overlain by red laminated siltstone (Red Shale Member of the Mount Doreen Formation). In both cases, in our view, the barite horizon marks a conformable transition from deposition under the influence of storm waves (i.e. size-sorted peloids, low-angle crossbedding) to sedimentation below the storm wave base. Walter & Bauld (1983) suggested that the barite was secondary after primary anhydrite ($CaSO_4$), contingent on their interpretation that the carbonate and sulphate were products of intense evaporation in glacial lakes such as those of the Antarctic Dry Valleys. This is not a credible scenario in an open marine setting in the absence of a local hydrothermal source of Ca.

Seafloor barite in northwestern Canada. In the Mackenzie Mountains of northwestern Canada, the top 4–10 cm of the Ravensthroat cap dolostone contains digitate barite cement (variably calcitized) over a strike length of nearly 200 km (Hoffman & Halverson 2011). The barite coincides with a change in colour of the peloidal dolostone from pale cream to chocolate brown. Locally, the barite-rich layer is developed on a train of giant wave ripples. The barite first appears as randomly oriented, millimetre-scale, bladed crystals, which appear to have formed just below the sediment–water interface. Upwards, the crystals self-organize to form centimetre-scale digitate structures, commonly oversteepened toward the SW (seaward). The digitate structures display coral-like growth laminae, defined by films of opaque minerals. Where calcitized, they resemble microdigitate stromatolites except for their diagnostic bladed crystal habit (so-called barite 'rosettes'). The flanks of the digitate structures are ragged due to outward growth of barite after each lamina of peloidal Fe-dolomite was deposited between the digits. The interplay between crystal growth and burial by peloids demonstrates that the barite precipitated from the water column, into which the digitate structures projected up to 1.0 cm above the seafloor. The Fe-dolostone layer with barite cement makes a conformable contact with overlying micritic limestone (Hayhook Formation) – epigenetically dolomitized locally – containing acicular crystal fans of pseudomorphosed aragonite cement and reworked detrital dolomite basally (James *et al.* 2001).

Early diagenetic barite in the Taoudeni Basin, West Africa. The common occurrence of barite in cap dolostones terminating the Jbéliat glaciation of the West African craton has been known for half a century (Deynoux & Trompette 1981). The type area is the Atar Cliff, Mauritania, on the northern edge of the Taoudeni Basin (Fig. 5.3). There, the cap dolostone directly overlies a periglacial permafrost regolith with deep polygonal sand wedges, developed above a terrestrial sub- and proglacial succession of northerly derivation and vast extent (Deynoux 1982, 1985; Deynoux *et al.* 2006). The cap dolostone is variably brecciated and spectacular metre-scale tepee structures (Kendall & Warren 1987) are developed toward the top near Amogjar, east of Atar. Isopachous barite forms thick crusts around blocks of brecciated dolostone, as well as secondary (remobilized?) vein-fillings (Shields *et al.* 2007). An early diagenetic origin for the cavity-filling, crustose barite is indicated by detrital barite clasts in coarse-grained quartz sand- and granulestone of the cap-carbonate sequence highstand tract (Fig. 5.3).

Early diagenetic barite on the Yangtze Platform, South China. A relatively thin (2.5–4.0 m) cap dolostone (lower Doushantuo Formation units C1–3 of Jiang *et al.* 2006) blankets terminal Cryogenian (Marinoan) glaciogenic deposits of the Nantuo Formation on the Yangtze platform (Jiang *et al.* 2006). Void-filling barite fans occur in the lower part (unit C1) of the cap dolostone on the inner platform and on the slope and basin to the SE. Unit 1 is brecciated everywhere and hosts a variety of sheet-crack cements, cement-filled stromatactis-like cavities, and tepee-like structures (Jiang *et al.* 2006). Importantly, the base of unit C1 is a sharp, smooth, undulating surface; neither it nor the upper Nantuo Formation experienced the intense brecciation typically observed within unit C1 (Jiang *et al.* 2006). In addition, possible seafloor barite is described as 'layer-parallel barite fans growing out of the dolomicrite substrate' in the lower part of unit C2 in the basin (Jiang *et al.* 2006). Tepee-like structures occur locally in the lower part of unit C2 on the platform. Unit 3 and the upper part of unit C2 are not brecciated, consisting of parallel- and small-scale cross-laminated peloidal dolopackstone with graded layers. Unit 3 has increased silt and limestone (Jiang *et al.* 2006).

Early diagenetic barite on the Dzabkhan Platform, western Mongolia. A characteristic Marinoan cap dolostone (Table 5.2) overlies the younger of two Cryogenian glaciogenic horizons (Khongoryn diamictite) on the Dzabkhan platform of western Mongolia (Macdonald *et al.* 2009, 2011). Barite occurs in the mountain pass (Hoh Davaa) between Bayan-Uul and Jargalan in northern Govi-Altay. There the cap dolostone includes two units, separated by a sharp smooth disconformity veneered by dark brown Fe-dolostone. The first unit (11.1 m) is a pale tan peloidal dolostone with low-angle crossbedding. Isopachous sheet-crack cements occur near its base, above the basal 0.7 m of marly brown ribbon beds. The second unit (8.4 m) consists of variably brecciated medium-grey dolostone with thick crusts of isopachous void-filling barite cement. Toward the top, sheet-crack and stratiform barites form domal structures with up to 1.0 m of relief. The barite domes were ultimately onlapped and buried by a third unit consisting of unbrecciated medium-dark grey dolostone ribbons with subaqueous microbial textured intervals, including rollup structures, that lead into the scree-covered maximum flooding horizon of the Ol cap-carbonate sequence. Although onlap relations clearly show that the domal barite was exposed to seawater at the top of the second unit, proof that it formed on the seafloor in the form of detailed interaction between sedimentation and precipitation has yet to be observed.

Phosphorite in cap-carbonate sequences

Taoudeni Basin, West Africa

On the northeastern margin of the Taoudeni Basin, diamictite of the Jbéliat glaciation (Fersiga Formation) is overlain by a cap-carbonate sequence correlative with that found in palaeovalleys on the Atar Cliffs (Fig. 5.3), 1250 km to the SW (Bertrand-Sarfati *et al.* 1997; Deynoux *et al.* 2006). A thin but continuous cap dolostone (Oued Djouf Formation) is overlain by a regressive highstand sequence (Grizim Formation) up to 80 m thick, composed of glauconitic green shale, siltstone and sandstone, ultimately aeolian (Bertrand-Sarfati *et al.* 1997). Apatitic phosphorite is concentrated at the base of the Grizim Formation, forming stromatolitic domes, microdigitate clusters and shrub-like colonies over moraines of Fersiga diamictite, where the cap dolostone is brecciated due to subaerial exposure, and crossbedded phospharenite composed of phosphate-coated grains and oncolites in the inter-moraine depressions (Bertrand-Sarfati *et al.* 1997). Authigenic glauconite occurs in both phosphorite facies and void-filling barite is a minor constituent of the shrub-like phosphate colonies. The phosphorites formed rapidly, during the initial stages of the glacio-eustatic transgression (Bertrand-Sarfati *et al.* 1997).

Phosphorites of early Ediacaran age occur in other areas, but their connection to glaciation is tenuous. Khodjari-type

phosphorite in the northern Volta basin was tentatively linked to the terminal Cryogenian deglaciation of West Africa (Trompette *et al.* 1980), but the phosphorite is younger than regionally extensive silicified green argillite ('silexite'), which itself disconformably overlies the basal Ediacaran (Marinoan) cap-carbonate sequence in the Taoudeni basin (Fig. 5.3; Bertrand-Sarfati *et al.* 1997; Shields *et al.* 2007). Similarly, economic phosphorite in the Khubsugul area of northern Mongolia (Ilyin *et al.* 1986) was genetically related to the underlying terminal Cryogenian Khesen diamictite (Sheldon 1984). However, Ilyin (2009) and recent mapping has shown that the phosphorite is separated from post-glacial Baxha cap-carbonate sequence by a major hiatus (Macdonald & Jones 2011).

Genesis and significance of glacial-associated chemical sediments

Fe and Fe–Mn oxide deposits

Ferrous v. euxinic anoxia. Anoxia due to ice cover has long been invoked as a means of mobilizing reduced Fe and Mn in solution as a source for oxide ores within Cryogenian glaciogenic sequences (Martin 1965*b*; Urban *et al.* 1992; Klein & Beukes 1993; Lottermoser & Ashley 2000; Klein & Ladeira 2004). Fe(II) concentration in the presence of H_2S is limited by pyrite (FeS_2) saturation. High degrees of continental ice cover and consequent large sea-level falls favour Fe over S in ocean waters because of reduced riverine sulphate supply and higher Fe/S in deep-sea hydrothermal vent fluids, respectively (Canfield & Raiswell 1999; Kump & Seyfried 2005).

Subglacial sulphate-rich ferrous waters. The discovery of modern Fe- and sulphate-rich (3.45 and 50 mM, respectively) waters trapped beneath the Taylor Glacier in the McMurdo Dry Valleys of East Antarctica gives a new perspective on Cryogenian jaspilites (Mikucki *et al.* 2009). Fe is not titrated as pyrite because there is insufficient organic primary production, due to the glacier cover, to fuel bacterial sulphate reduction. The source of Fe in the trapped former seawater is subaqueous bedrock 'weathering', enhanced by the low pH (6.2) of the waters. Fe-oxy-hydroxide forms instantaneously at Blood Falls, where the anoxic waters discharge at the glacier terminus (Mikucki *et al.* 2009). This demonstrates that waters rich in both dissolved Fe and sulphate can exist if ice cover is perennial and sufficiently thick to preclude phototrophic primary production.

Localization of oxidative titration. In anoxic Fe-rich waters, the localization of Fe (and Mn) deposition could relate to the availability of oxygenated subglacial meltwater at the grounding-lines of wet-base ice streams within cold-base ice sheets. This would be consistent with the observed occurrence of Cryogenian jaspilites as lenticular bodies in contact with diamictite complexes whose lithofacies and internal organization is most consistent with deposition in ice-sheet grounding zones. Alternation of Fe and Mn ores could relate to variations of the meltwater flux associated with glacial retreat and advance, respectively, as proposed by Urban *et al.* (1992).

Cap-carbonate sequences

Accumulation rates for syndeglacial cap dolostones. Marinoan cap dolostones were deposited during marine transgressions resulting from the meltdown of grounded ice sheets (Preiss *et al.*, 1978; Kennedy 1996; Bertrand-Sarfati 1997; James *et al.* 2001; Shields 2005; Fairchild & Kennedy 2007; Hoffman *et al.* 2007). The timescales for Cryogenian deglaciations have not been specifically targeted in climate modelling. Nevertheless, deglaciation histories of the temperate Quaternary ice sheets, simplified Neoproterozoic deglacial simulations, and the apparent absence of polar continents in Cryogenian palaeogeographic reconstructions (Fig. 5.1) all suggest that Sturtian and Marinoan ice sheets disappeared rapidly. How rapidly? If those middle and low-latitude ice sheets disappeared at the rate most temperate mountain glaciers have been lowered in recent decades ($\sim$1.1 m/a), their demise would have taken $\sim$2 ka assuming their average thickness was comparable with the present East Antarctic Ice Sheet (Lythe *et al.* 2001). This is close to the pan-deglacial timescale of $<$2 ka in a climate model (Hyde *et al.* 2000). Positive feedbacks – ice-albedo, ice-elevation and various greenhouse-gas feedbacks notably water vapour feedback – contribute to rapid deglaciation. The energy demands for such a deglaciation, amounting to a globally averaged energy flux of *c.* 11 W m^2 (Wallace & Hobbs 1977, p. 320), are small compared to the Neoproterozoic solar irradiance of *c.* 362 W m^2 (*c.* 94% of present), a high surface albedo notwithstanding. Pending detailed modelling of a global deglaciation, we conservatively take 8 ka, the timescale for Quaternary deglaciations, as an upper limit for the Marinoan deglaciation. Given median (9 m) and maximum (175 m) thicknesses of Marinoan cap dolostones globally (Hoffman *et al.* 2007), average accumulation rates were then *c.* 1 and 22 mm/a for cap dolostones of typical and extreme thickness, respectively. If deglaciation occurred in 2 ka, the respective accumulation rates were four times larger. These must be considered minimum rates, as cap dolostones at any given location represent only a fraction of the total deglaciation (Fig. 5.2). We consider it likely that unusual structures in cap dolostones (e.g. sheet-crack cements, tubestone stromatolites and highly aggradational wave ripples) may be fundamentally related to extreme rates of accumulation.

The record of geomagnetic reversals and excursions in the Mirassol d'Oeste and Nuccaleena cap dolostones creates a dilemma (Trindade *et al.* 2003; Raub 2008). Conventional estimates of their duration and frequency (Johnson *et al.* 1995; Gubbins 1999; Roberts 2008) imply a timescale on the order of 0.1–1.0 Ma for those cap dolostones, implying that accumulation rates were at least 10–100 times slower than the 'conservative' estimates given in the preceding paragraph. This makes for an irreconcilable conflict between conventional interpretations of geomagnetic polarity reversals and excursions on the one hand, and estimated deglaciation rates on the other. If one accepts a conventional magnetostratigraphic interpretation, cap dolostones are highly condensed (Fairchild & Kennedy 2007). However, compared with other depositional sequences in the same (or other) successions, Marinoan cap dolostones are relatively thick and expanded among transgressive tracts (e.g. Hoffman & Halverson 2008). The resolution of geomagnetic field reversals and excursions is limited by the accumulation rates of the sediments in which the records are kept (Channell & Lehman 1997; Roberts & Lewin-Harris 2000; Roberts 2008). If Marinoan cap dolostones were actually deposited at rates far exceeding the best Quaternary deep-sea records (Channell & Lehman 1997; Laj *et al.* 2006), might they not display hitherto unsuspected phenomena? This would most likely be the case if the absolute strength of the geomagnetic field was collapsed in 635 Ma, just as it does during field reversals and excursions. The slowness with which the solid inner core reverses, by diffusion, does not limit the speed with which the outer core alone reverses in a weak field (Gubbins 1999). In our view, the issue is unresolved, but neither the sedimentological evidence for high sedimentation rates nor the physical arguments for rapid deglaciation should be dismissed lightly.

Are syndeglacial cap dolostones non-marine?

If Marinoan ice sheets had an average thickness of *c.* 2.2 km over all continents and shelves (Fig. 5.1), their disappearance in 10 ka

would produce meltwater at a global average rate of *c.* 0.6×10^6 m^3 s^{-1} (2.01×10^{17} m^3/3.15×10^{10} s), or *c.* 6.4 Sv (Sverdrups, where 1.0 Sv $= 10^6$ m^3 s^{-1}). Deglaciation in 2 ka would result in a global meltwater flux of *c.* 32 Sv. These values correspond to approximately 6 and 32 times present total runoff, respectively. Such an increase in freshwater input, followed by strong surface warming after the ice disappeared, must have impeded ocean mixing by creating a more stable density stratification (Shields 2005). Cold saline deepwater that evolved during the Marinoan glaciation would have been capped by a thickening meltwater-dominated lid. The melting of sea ice, or a sea glacier in the case of a Snowball Earth (Warren *et al.* 2002; Goodman & Pierrehumbert 2003), followed by the melting of ice sheets, would have contributed up to 0.7 and *c.* 1.0 km of freshwater respectively. Ocean mixing time would have been many times the present 10^3 years, ensuring that the surface ocean was brackish when cap dolostones were deposited (Shields 2005). This meltwater-dominated lid has been dubbed 'plumeworld' (Shields 2005), and we refer to the Marinoan example as 'Glacial Lake Harland' (GLH). (W. Brian Harland of Cambridge University was a pioneer advocate of Neoproterozoic glaciations as chronostratigraphic markers.) Shields (2005, p. 305) gives many reasons why GLH was more favourable than seawater for rapid carbonate production.

Abiotic or biogenic dolomite?

The dolomicrospar of cap dolostones preserves primary structures, makes conformable contact with overlying and (rare) underlying limestones, and near the base of the former is reworked as intraclastic dolomite grains. These are good reasons to conclude that the dolomite was either primary or a product of very early diagenesis near the sediment–water interface. It has recently been demonstrated that dolomite-forming reactions are catalysed at low temperatures by microbial activity utilizing different metabolic pathways: sulphate reduction (van Lith *et al.* 2003), anaerobic methane oxidation (Moore *et al.* 2004) and methanogenesis by Archaea (Kenward *et al.* 2009). The first of these has been applied to Marinoan cap dolostones (Shields 2005; Font *et al.* 2006; Nédélec *et al.* 2007). However, methanogenesis by Archaea is particularly appealing because the formation of ordered dolomite at low temperature (4°C) has been demonstrated experimentally in a low sulphate, low Mg:Ca (<1), acidic (pH = 6.7), freshwater environment, not unlike GLH (see above). As the methanogenic consortium (Kenward *et al.* 2009) is anaerobic, formation of cap dolostone by this means must have occurred below the sediment–water interface, assuming deglacial surface waters were well oxygenated.

Sources of alkalinity for cap dolostones. Syndeglacial carbonate production in surface waters was driven by warming ($\Delta T \approx 50$°C; Pierrehumbert 2002), inundation of shallow shelves and platforms where carbonate burial is favoured (Ridgwell *et al.* 2003), alkalinity provided by anaerobic respiration (Kennedy *et al.* 2001; but see Shields 2005 for critical discussion), and carbonate weathering (Higgins & Schrag 2003; Anderson 2007; see Le Hir *et al.* 2009 for critical discussion, but note that they consider only silicate weathering as a source of alkalinity, not carbonate weathering which is orders of magnitude more rapid).

Significance of seafloor aragonite cements. Seafloor cements composed of former aragonite occurring in limestones above Marinoan cap dolostones formed below the storm wave base, at or near the maximum flooding horizon (Grotzinger & Knoll 1995; James *et al.* 2001; Nogueira *et al.* 2003; Hoffman 2011). They represent a brief revival of more ancient conditions following a long decline in the importance of seafloor cement in the latter half of the Proterozoic (Grotzinger & James 2000; Sumner 2002). What was the source of alkalinity driving carbonate production in deep water? One possibility is anaerobic respiration, which operates as an alkalinity pump in modern super-anoxic fjords (Anderson *et al.* 1987). Another is that extreme concentrations of dissolved inorganic carbon (DIC), expected for an ocean equilibrated with carbonate sediments and a *c.* 0.1 bar CO_2 atmosphere, flattened the negative gradient in carbonate saturation (Ω) with increasing depth, favouring the precipitation of cement on the seafloor, irrespective of the oxidant or intensity of organic carbon cycling (Higgins *et al.* 2009).

Barite in cap dolostones

Seafloor barite. Seafloor barites in basal Ediacaran (Marinoan) cap dolostones of central Australia and northwestern Canada are strikingly similar in form, dimensions and precise stratigraphic position within their respective cap-carbonate sequences. We infer that they formed where the seabed intersected the interface between Ba-rich euxinic deeper water and an oxic Fe(III)-laden mixed layer. Localized upwelling would then have caused sulphate production and barite titration. Simultaneously, anaerobic respiration, where Fe was the electron acceptor, caused Fe(III) reduction, leading to Fe-carbonate (Fe-dolostone) production coincident with the barite cement horizon. It is well established that mixed-layer waters from which cap dolostones were deposited were Fe(III)-laden (Embleton & Williams 1986; Li 2000; Font *et al.* 2005), accounting for the pinkish tint of many cap dolostones. Ba in euxinic glacial deep waters would derive from seawater–basalt exchange reactions and seafloor weathering of detrital feldspar. We see no need for the involvement of methane venting, for which there is neither physical nor isotopic evidence at seafloor barite horizons in Marinoan cap dolostones (Kennedy 1996; Hoffman & Halverson 2011). Euxinic deep water that evolved during the Marinoan glaciation (Hurtgen *et al.* 2006) may have contrasted with Fe(II) sulphate deep water (Mikucki *et al.* 2009), which may have developed during the Sturtian glaciation, accounting for the deposition of haematite–jaspilite at that time.

Early diagenetic (void-filling) barite. Tepee breccias in cap dolostones and associated void-filling isopachous barite cement have been ascribed to vadose diagenesis in West Africa (Bertrand-Sarfati *et al.* 1997; Shields *et al.* 2007). In South China, similar features have been attributed to submarine cold seeps (Jiang *et al.* 2006) or, alternatively, to vadose diagenesis (Zhou *et al.* 2010). In both interpretations, barite precipitation is thought to have resulted from mixing of an oxic sulphate-rich fluid (seawater) and a highly reducing, Ba- and possibly methane-rich fluid, derived from the destabilization of permafrost gas hydrate in underlying glaciogenic sediments from which the Ba was scavenged (Jiang *et al.* 2006; Shields *et al.* 2007). It remains to be seen if this attractive scenario is compatible with a basic field observation in both areas, that the contact surface between the glaciogenic diamictite and the cap dolostone is smooth and unbroken (authors' observations). Is it conceivable that methane and other gases, generated within the till (permafrost melting), could thoroughly brecciate the cap dolostone on the seafloor, while leaving their mutual contact surface undisturbed? Methane involvement is supported by extreme δ^{13}C depletion (below −10‰ Vienna Pee Dee Belemnite standard) in certain void-filling cement phases in brecciated cap dolostone on the Yangtze platform (Jiang *et al.* 2003; Wang *et al.* 2008). However, such strong depletions are not observed elsewhere, despite thousands of published analyses, and those in South China come mostly from late-stage calcite void-fillings that demonstrably post-date coexisting barite and void-filling dolomite cements (Zhou *et al.* 2011). Moreover, δ^{34}S values in cap dolostones are not strongly enriched, as predicted if anaerobic methane oxidation (an alkalinity pump) was fueling bacterial sulphate reduction (Shields 2005).

Phosphorite in cap dolostones

It is not possible to generalize about Neoproterozoic glacial-related phosphorite from a single example, no matter how impressive and well documented it is (Bertrand-Sarfati *et al.* 1997). Its existence supports assumed high productivity during deglaciation (Shields 2005; Font *et al.* 2006; Nédélec *et al.* 2007).

Conclusions

Synglacial Fe and Fe–Mn deposits are mostly, if not all, associated with the older Cryogenian (Sturtian) glaciation. They indicate anoxic (not euxinic) deep water. Lithofacies associations suggest that subglacial meltwater plumes provided oxidant. Alternating Fe and Mn deposits may reflect oscillating plume fluxes associated with glacial cycles.

Sturtian and Marinoan cap carbonates are distinct. Transgressive cap dolostones are almost entirely limited to the Marinoan deglaciation, and were deposited diachronously, mainly above the storm wave base, during coastal inundation by meltwater-dominated surface waters. Biogenic dolomite nucleation in waters of low ionic strength and low Mg:Ca ratio was likely microbially mediated.

Barite occurs in Marinoan cap dolostones both as seafloor cements in terminal Fe-dolomite beds and as early diagenetic void-filling crusts within tepee and tepee-like breccias. Seafloor barite cement formed where euxinic Ba-rich deep waters upwelled into oxic Fe(III)-rich surface waters. Early diagenetic void-filling barite cement in cap dolostones has been attributed to subaerial and submarine methane seepage, driven by destabilization of permafrost hydrates in underlying sediments following marine inundation. Although attractive in principle, undisturbed contact surfaces between glaciogenic diamictites and internally brecciated cap dolostones may be difficult to reconcile with seepage from below, unless brecciation was strictly limited to the horizon of methane oxidation.

Fieldwork was supported by research grants from the Earth System History (ESH), Arctic Natural Science (ANS), and Geobiology & Environmental Geochemistry (GEG) programmes of the US National Science Foundation (NSF). PFH receives additional support from the Canadian Institute for Advanced Research (CIFAR), Harvard University Center for the Environment (HUCE), US Social Security, and the Canada Pension Plan. FAM and GPH thank the Yukon Geological Survey for additional support. We gratefully acknowledge constructive reviews by G. Jiang and P. K. Link, which prompted several improvements. This represents a contribution of the IUGS- and UNESCO-funded IGCP (International Geoscience Programme) Project #512.

References

Aitken, J. D. 1991. The Ice Brook Formation and post-Rapitan, late Proterozoic glaciation, Mackenzie Mountains, Northwest Territories. *Geological Survey of Canada Bulletin*, **404**, 1–43.

Allen, P. A. & Hoffman, P. F. 2005. Extreme winds and waves in the aftermath of a Neoproterozoic glaciation. *Nature*, **433**, 123–127.

Allen, P., Leather, J. & Brasier, M. D. 2004. The Neoproterozoic Fiq glaciation and its aftermath, Huqf Supergroup of Oman. *Basin Research*, **16**, 507–534.

Alvarenga, C. J. S. de & Trompette, R. 1992. Glacially influenced sedimentation in the Later Proterozoic of the Paraguay belt (Mato Grosso, Brazil). *Palaeogeography, Palaeoclimatology, Palaeoecology*, **92**, 85–105.

Alvarenga, C. J. S. de, Dardenne, M. A. *et al.* 2008. Isotope stratigraphy of Neoproterozoic cap carbonates in the Araras Group, Brazil. *Gondwana Research*, **13**, 469–479.

Anderson, J. B. 1999. *Antarctic Marine Geology*. Cambridge University Press, Cambridge.

Anderson, S. P. 2007. Biogeochemistry of glacial landscape systems. *Annual Review of Earth and Planetary Sciences*, **35**, 375–399.

Anderson, L. G., Dyrssen, D. & Skei, J. 1987. Formation of chemogenic calcite in super-anoxic seawater–Framvaren, Southern-Norway. *Marine Chemistry*, **20**, 361–376.

Assereto, R. L. A. M. & Kendall, C. G. St. C. 1977. Nature, origin and classification of peritidal tepee structures and related breccas. *Sedimentology*, **24**, 153–210.

Badenhorst, F. P. 1988. The lithostratigraphy of the Chuos mixtite in part of the southern central zone of the Damara Orogen, South West Africa. *Communications of the Geological Survey of South West Africa/Namibia*, **4**, 103–110.

Bao, H., Lyons, J. R. & Zhou, C. 2008. Triple oxygen isotope evidence for elevated CO_2 levels after a Neoproterozoic glaciation. *Nature*, **452**, 504–506.

Bertrand-Sarfati, J., Flicoteaux, R., Moussine-Pouchkine, A. & Aït Kaci Ahmed, A. 1997. Lower Cambrian apatitic stromatolites and phospharenites related to the glacio-eustatic cratonic rebound (Sahara, Algeria). *Journal of Sedimentary Research*, **67**, 957–974.

Cahen, L. & Lepersonne, J. 1981. Proterozoic diamictites of Lower Zaire. *In*: Hambrey, M. J. & Harland, W. B. (eds) *Earth's Pre-Pleistocene Glacial Record*. Cambridge University Press, Cambridge, 153–157.

Cahen, L. 1950. Le Calcaire de Sekelolo, le Complexe tillitique et la Dolomie rose C_1 dans l'Anticlinal de Congo dia Kati (Bas-Congo). *Annales du Musée du Congo Belge, Sciences Géologiques*, **7**, 13–54.

Calver, C. R. & Walter, M. R. 2000. The late Neoproterozoic Grassy Group of King Island, Tasmania: correlation and palaeogeographic significance. *Precambrian Research*, **100**, 299–312.

Canfield, D. E. & Raiswell, R. 1999. The evolution of the sulfur cycle. *American Journal of Science*, **299**, 697–723.

Channell, J. E. T. & Lehman, B. 1997. The last two geomagnetic polarity reversals recorded in high-deposition-rate sediment drifts. *Nature*, **389**, 712–715.

Chumakov, N. M. 1992. The problems of old glaciations: Pre-Pleistocene glaciogeology in the USSR. *Soviet Science Reviews, Section G Geology*, **1**, 1–208.

Chumakov, N. M. 2007. Climates and climate zonality of the Vendian: geological evidence. *In*: Vickers-Rich, P. & Komarower, P. (eds) *The Rise and Fall of the Ediacaran Biota*. Geological Society, London, Special Publication, **286**, 15–26.

Clifford, T. N. 2008. The geology of the Neoproterozoic Swakop–Otavi transition zone in the Outjo Distroct, northern Damara Orogen, Namibia. *South African Journal of Geology*, **111**, 117–140.

Cloud, P., Wright, L. A., Williams, E. G., Diehl, P. & Walter, M. R. 1974. Giant stromatolites and associated vertical tubes from the upper Proterozoic Noonday Dolomite, Death Valley region, eastern California. *Geological Society of America Bulletin*, **85**, 1869–1882.

Condon, D., Zhu, M., Bowring, S. A., Wang, W., Yang, A. & Jin, Y. 2005. U–Pb ages from the Neoproterozoic Doushantuo Formation, China. *Science*, **308**, 95–98.

Corkeron, M. 2007. 'Cap carbonates' and Neoproterozoic glacigenic successions from the Kimberley region, north-west Australia. *Sedimentology*, **54**, 871–903.

Corkeron, M. L. & George, A. D. 2001. Glacial incursion on a Neoproterozoic carbonate platform in the Kimberley region, Australia. *Geological Society of America Bulletin*, **113**, 1121–1132.

Corsetti, F. A. & Grotzinger, J. P. 2005. Origin and significance of tube structures in Neoproterozoic post-glacial cap carbonates: example from Noonday Dolomite, Death Valley, United States. *Palaios*, **20**, 348–363.

Corsetti, F. A. & Kaufman, A. J. 2003. Stratigraphic investigations of carbon isotope anomalies and Neoproterozoic ice ages in Death Valley, California. *Geological Society of America Bulletin*, **115**, 916–932.

Deynoux, M. 1982. Periglacial polygonal structures and sand wedges in the late Precambrian glacial formations of the Taoudeni Basin in Adrar of Mauretania (West Africa). *Palaeogeography, Palaeoclimatology, Palaeoecology*, **39**, 55–70.

Deynoux, M. 1985. Terrestrial or waterlain glacial diamictites? Three case studies from the late Proterozoic and late Ordovician glacial drifts in West Africa. *Palaeogeography, Palaeoclimatology, Palaeoecology*, **51**, 97–141.

Deynoux, M. & Trompette, R. 1976. Discussion: Late Precambrian mixtites: glacial and/or nonglacial? Dealing especially with the mixtites of West Africa. *American Journal of Science*, **276**, 1302–1315.

Deynoux, M. & Trompette, R. 1981. Late Precambrian tillites of the Taoudeni Basin, West Africa. *In*: Hambrey, M. J. & Harland, W. B. (eds) *Earth's Pre-Pleistocene Glacial Record*. Cambridge University Press, Cambridge, 123–131.

Deynoux, M., Affaton, P., Trompette, R. & Villeneuve, M. 2006. Pan-African tectonic evolution and glacial events registered in Neoproterozoic to Cambrian cratonic and foreland basins of West Africa. *Journal of African Earth Sciences*, **46**, 397–426.

Dorr, J. V. N. II. 1945. Manganese and iron deposits of Morro do Urucum, Mato Grosso, Brazil. *United States Geological Survey Bulletin*, **946-A**, 1–47.

Dowdeswell, J. A., Whittington, J. A., Jennings, A. E., Andrews, J. T., Mackensen, A. & Marienfield, P. 2000. An origin for laminated glacimarine sediments through sea-ice build-up and suppressed iceberg rafting. *Sedimentology*, **47**, 557–576.

Dunn, P. R., Thompson, B. P. & Rankama, K. 1971. Late Pre-Cambrian glaciation in Australia as a stratigraphic boundary. *Nature*, **231**, 498–502.

Edwards, M. B. 1984. Sedimentology of the Upper Proterozoic glacial record, Vestertana Group, Finnmark, North Norway. *Norges Geologiske Undersøkelse Bulletin*, **394**, 76.

Eisbacher, G. H. 1985. Late Proterozoic rifting, glacial sedimentation and sedimentary cycles in the light of Windermere deposition, western Canada. *Palaeogeography, Palaeoclimatology, Palaeoecology*, **51**, 231–254.

Embleton, B. J. J. & Williams, G. E. 1986. Low latitude of deposition for late Precambrian periglacial varvites in South Australia: implications for palaeoclimatology. *Earth and Planetary Science Letters*, **79**, 419–430.

Fairchild, I. J. & Kennedy, M. J. 2007. Neoproterozoic glaciation in the Earth System. *Journal of the Geological Society, London*, **164**, 895–921.

Fanning, C. M. & Link, P. K. 2008. *Age constraints for the Sturtian glaciation: data from the Adelaide Geosyncline, South Australia and Pocatello Formation, Idaho, USA*. Selwyn Symposium 2008, Geological Society of Australia, Extended Abstracts, **91**, 57–62.

Fölling, P. G. & Frimmel, H. E. 2002. Chemostratigraphy correlation of carbonate successions in the Gariep and Saldania Belts, Namibia and South Africa. *Basin Research*, **14**, 69–88.

Fölling, P. G., Zartman, R. E. & Frimmel, H. E. 2000. A novel approach to double-spike Pb/Pb dating of carbonate rocks: examples from Neoproterozoic sequences in southern Africa. *Chemical Geology*, **171**, 97–122.

Font, E., Nédélec, A., Trindade, R. I. F., Macouin, M. & Charrière, A. 2006. Chemostratigraphy of the Neoproterozoic Mirassol d'Oeste cap dolostones (Mato Grosso, Brazil): an alternative model for Marinoan cap dolostone formation. *Earth and Planetary Science Letters*, **250**, 89–103.

Font, E., Trindade, R. I. F. & Nédélec, A. 2005. Detrital remanent magnetization in haematite-bearing Neoproterozoic Puga cap dolostone, Amazon craton: a rock magnetic and SEM study. *Geophysical Journal International*, **163**, 491–500.

Frimmel, H. E. 2004. Neoproterozoic sedimentation rates and timing of glaciations – a southern African perspective. *In*: Eriksson, P. G., Altermann, W., Nelson, D. R., Mueller, W. U. & Catuneanu, O. (eds) *The Precambrian Earth: Tempos and Events*. Elsevier, Amsterdam, 459–473.

Frimmel, H. E. 2008. Neoproterozoic Gariep Orogen. *In*: Miller, R. McG. (ed.) *The Geology of Namibia (In Three Volumes), Volume 2 (Neoproterozoic to Lower Palaeozoic)*. Geological Survey of Namibia, Windhoek, 14-1–14-39.

Frimmel, H. E. & Von Veh, M. W. 2003. Numees formation (including the Jakkalsberg Member). *In*: Johnson, M. R. (ed.) *Catalogue of South African Lithostratigraphic Units*. South African Committee for Stratigraphy, Pretoria, 7-25–7-28.

Frimmel, H. E. 2011. The Kaigas and Numees Formations, Port Nolloth Group, in South Africa and Namibia. *In*: Arnaud, E., Halverson, G. P. & Shields-Zhou, G. (eds) *The Geological Record of Neoproterozoic Glaciations*. Geological Society, London, Memoirs, **36**, 223–231.

Gammon, P. R., McKirdy, D. M. & Smith, H. D. 2005. The timing and environment of tepee formation in a Marinoan cap carbonate. *Sedimentary Geology*, **177**, 195–208.

Gaucher, C., Frimmel, H. E. & Germs, G. J. B. 2005. Organic-walled microfossils and biostratigraphy of the upper Port Nolloth Group (Namibia): implications for latest Neoproterozoic glaciations. *Geological Magazine*, **142**, 539–559.

Goodman, J. & Pierrehumbert, R. T. 2003. Glacial flow of floating marine ice in 'Snowball Earth'. *Journal of Geophysical Research*, **108**, 3308, doi: 10.1029/2002JC001471.

Graf, J. L., Jr, O'Connor, E. A. & Van Leeuwin, P. 1994. Rare earth element evidence of origin and depositional environment of Late Proterozoic ironstone beds and manganese-oxide deposits, SW Brazil and SE Bolivia. *Journal of South American Earth Sciences*, **7**, 115–133.

Grotzinger, J. P. & James, N. P. 2000. Precambrian carbonates: evolution of understanding. *In*: Grotzinger, J. P. & James, N. P. (eds) *Carbonate Sedimentation and Diagenesis in the Evolving Precambrian World*. SEPM (Society for Sedimentary Geology) Special Publication, **67**, 3–20.

Grotzinger, J. P. & Knoll, A. H. 1995. Anomalous carbonate precipitates: is the Precambrian the key to the Permian? *Palaios*, **10**, 578–596.

Gubbins, D. 1999. The distinction between geomagnetic excursions and reversals. *Geophysical Journal International*, **137**, F1–F3.

Halverson, G. P. & Shields, G. 2011. Chemostratigraphy and the Neoproterozoic glaciations. *In*: Arnaud, E., Halverson, G. P. & Shields, G. (eds) *The Geological Record of Neoproterozoic Glaciations*. Geological Society, London, Memoirs, **36**, 51–66.

Halverson, G. P., Maloof, A. C. & Hoffman, P. F. 2004. The Marinoan glaciation (Neoproterozoic) in northeast Svalbard. *Basin Research*, **16**, 297–324.

Halverson, G. P., Hoffman, P. F., Schrag, D. P., Maloof, A. C. & Rice, A. H. N. 2005. Toward a Neoproterozoic composite carbon-isotope record. *Geological Society of America Bulletin*, **117**, 1181–1207.

Halverson, G. P., Dudás, F. Ö., Maloof, A. C. & Bowring, S. A. 2007. Evolution of the $^{87}Sr/^{86}Sr$ composition of Neoproterozoic seawater. *Palaeogeography, Palaeoclimatology, Palaeoecology*, **256**, 103–129.

Hegenberger, W. 1993. Stratigraphy and sedimentology of the Late Precambrian Witvlei and Nama Groups, East of Windhoek. *Geological Survey of Namibia Memoir*, **17**, 82.

Higgins, J. A. & Schrag, D. P. 2003. Aftermath of a snowball Earth. *Geophysics, Geochemistry, Geosystems*, **4**, doi:10.1029/2002GC000403.

Higgins, J. A., Fischer, W. W. & Schrag, D. P. 2009. Oxygenation of the ocean and sediments: consequences for the seafloor carbonate factory. *Earth and Planetary Science Letters*, **284**, 25–33.

Hildebrand, R. S. 2009. *Did westward subduction cause Cretaceous–Tertiary orogeny in the North American Cordillera?* Geological Society of America, Special Paper, **457**, 71.

Hoffman, P. F. 2011. Strange bedfellows: glacial diamictite and cap carbonate from the Marinoan (635 Ma) glaciation in Namibia. *Sedimentology*, 58–119.

Hoffman, P. F. & Halverson, G. P. 2008. Otavi group of the western northern platform, the eastern Kaoko Zone and the western northern Margin Zone. *In*: Miller, R. McG. (ed.) *The Geology of Namibia, Vol. 2: Neoproterozoic to Lower Palaeozoic*. Handbook of the Geological Survey of Namibia, Windhoek, 13.69–13.136.

Hoffman, P. F. & Halverson, G. P. 2011. Neoproterozoic glacial record in the Mackenzie Mountains, northern Canadian Cordillera. *In*: Arnaud, E., Halverson, G. P. & Shields, G. (eds) *The Geological Record of Neoproterozoic Glaciations*. Geological Society, London, Memoirs, **36**, 397–411.

Hoffman, P. F. & Li, Z. X. 2009. A palaeogeographic context for Neoproterozoic glaciation. *Palaeogeography, Palaeoclimatology, Palaeoecology*, **277**, 158–172.

Hoffman, P. F. & Macdonald, F. A. 2010. Sheet-crack cements and early regression in Marinoan (635 Ma) cap dolostones: regional

benchmarks of vanishing ice-sheets? *Earth and Planetary Science Letters*, **300**, 374–384.

Hoffman, P. F. & Schrag, D. P. 2002. The snowball Earth hypothesis: testing the limits of global change. *Terra Nova*, **14**, 129–155.

Hoffman, P. F., Kaufman, A. J., Halverson, G. P. & Schrag, D. P. 1998. A Neoproterozoic Snowball Earth. *Science*, **281**, 1342–1346.

Hoffmann, K.-H., Condon, D. J., Bowring, S. A. & Crowley, J. L. 2004. U–Pb zircon date from the Neoproterozoic Ghaub Formation, Namibia: constraints on Marinoan glaciation. *Geology*, **32**, 817–820.

Hoffman, P. F., Halverson, G. P., Domack, E. W., Husson, J. M., Higgins, J. A. & Schrag, D. P. 2007. Are basal Ediacaran (635 Ma) post-glacial 'cap dolostones' diachronous? *Earth and Planetary Science Letters*, **258**, 114–131.

Hurtgen, M. T., Halverson, G. P., Arthur, M. A. & Hoffman, P. F. 2006. Sulfur cycling in the aftermath of a 635-Ma snowball glaciation: evidence for a syn-glacial sulfidic deep ocean. *Earth and Planetary Science Letters*, **245**, 551–570.

Hyde, W. T., Crowley, T. J., Baum, S. K. & Peltier, W. R. 2000. Neoproterozoic 'snowball Earth' simulations with a coupled climate/ice-sheet model. *Nature*, **405**, 425–429.

Ilyin, A. V. 2009. Neoproterozoic banded iron formations. *Lithology and Mineral Resources*, **44**, 78–86.

Ilyin, A. V., Zaitsev, N. S. & Bjamba, Z. 1986. Khubsugul, Mongolia people's republic. *In*: Cook, P. J. & Shergold, J. H. (eds) *Phosphate Deposits of the World, Vol. 1: Proterozoic and Cambrian Phosphorites*. Cambridge University Press, Cambridge.

James, N. P., Narbonne, G. M. & Kyser, T. K. 2001. Late Neoproterozoic cap carbonates: Mackenzie Mountains, northwestern Canada: precipitation and global glacial meltdown. *Canadian Journal of Earth Sciences*, **38**, 1229–1262.

Jiafu, T., Heqin, F. & Zhioiu, G. 1987. Stratigraphy, type and formation conditions of the Late Precambrian banded iron ores in South China. *Chinese Journal of Geochemistry*, **6**, 332–351.

Jiang, G., Kennedy, M. J. & Christie-Blick, N. 2003. Stable isotopic evidence for methane seeps in Neoproterozoic postglacial cap carbonates. *Nature*, **426**, 822–826.

Jiang, G., Kennedy, M. J., Christie-Blick, N., Wu, H. & Zhang, S. 2006. Stratigraphy, sedimentary structures and textures of the late Neoproterozoic Doushantuo cap carbonate in South China. *Journal of Sedimentary Research*, **76**, 978–995.

Johnson, H. P., Van Patten, D., Tivey, M. & Sager, W. W. 1995. Geomagnetic polarity reversal rate for the Phanerozoic. *Geophysical Research Letters*, **22**, 231–234.

Kaufman, A. J., Jiang, G., Christie-Blick, N., Banerjee, D. M. & Rai, V. 2006. Stable isotope record of the terminal Neoproterozoic Krol platform in the Lesser Himalayas of northern India. *Precambrian Research*, **147**, 156–185.

Kendall, C. G. St. C. & Warren, J. 1987. A review of the origin and setting of tepees and their associated fabrics. *Sedimentology*, **34**, 1007–1027.

Kennedy, M. J. 1996. Stratigraphy, sedimentology and isotopic geochemistry of Australian Neoproterozoic postglacial cap dolostones: deglaciation, $\delta^{13}C$ excursions and carbonate precipitation. *Journal of Sedimentary Research*, **66**, 1050–1064.

Kennedy, M. J., Runnegar, B., Prave, A. R., Hoffmann, K.-H. & Arthur, M. A. 1998. Two of four Neoproterozoic glaciations? *Geology*, **26**, 1059–1063.

Kennedy, M. J., Christie-Blick, N. & Sohl, L. E. 2001. Are Proterozoic cap carbonates and isotopic excursions a record of gas hydrate destabilization following Earth's coldest intervals? *Geology*, **29**, 443–446.

Kenward, P. A., Goldstein, R. H., González, L. A. & Roberts, J. A. 2009. Precipitation of low-temperature dolomite from an aerobic microbial consortium: the role of methanogenic Archaea. *Geobiology*, **7**, 1–10.

Kianian, M. & Khakzad, A. 2008. *Geochemistry of glaciogenic Neoproterozoic banded iron-formations from Kerman District (Iran)*. 33rd International Geological Congress, Oslo, Abstracts, Session CGC-04.

Klein, C. 2005. Some Precambrian banded iron-formations (BIFs) from around the world: their age, geologic setting, mineralogy, metamorphism, geochemistry and origin. *American Mineralogist*, **90**, 1473–1499.

Klein, C. & Beukes, N. J. 1993. Sedimentology and geochemistry of the glacigenic Late Proterozoic Rapitan iron-formation in Canada. *Economic Geology*, **88**, 542–565.

Klein, C. & Ladeira, E. A. 2004. Geochemistry and mineralogy of Neoproterozoic banded iron-formations and some selected, siliceous manganese formations from the Urucum District, Mato Grosso do Sul, Brazil. *Economic Geology*, **99**, 1233–1244.

Knoll, A. H., Walter, M. R., Narbonne, G. M. & Christie-Blick, N. 2006. The Ediacaran Period: a new addition to the geologic time scale. *Lethaia*, **39**, 13–30.

Kump, L. R. & Seyfried, W. E. Jr. 2005. Hydrothermal Fe fluxes during the Precambrian: effect of low oceanic sulfate concentrations and low hydrostatic pressure on the composition of black smokers. *Earth and Planetary Science Letters*, **235**, 654–662.

Laj, C., Kissel, C. & Roberts, A. P. 2006. Geomagnetic field behavior during the Iceland Basin and Laschamp geomagnetic excursions: a simple transitional field geometry? *Geochemistry, Geophysics, Geosystems*, **7**, Q03004, doi:10.1029/2005GC001122.

Le Hir, G. & Donnadieu, Y. *et al.* 2009. The snowball Earth aftermath: exploring the limits of continental weathering processes. *Earth and Planetary Science Letters*, **277**, 453–463.

Li, Z. X. 2000. New palaeomagnetic results from the 'cap dolomite' of the Neoproterozoic Walsh Tillite, northwestern Australia. *Precambrian Research*, **100**, 359–370.

Li, Z. X. & Bogdanova, S. V. *et al.* 2008. Assembly, configuration and break-up history of Rodinia: a synthesis. *Precambrian Research*, **160**, 179–210.

Lottermoser, B. G. & Ashley, P. M. 2000. Geochemistry, petrology and origin of Neoproterozoic ironstones in the eastern part of the Adelaide Geosyncline. *Precambrian Research*, **101**, 49–67.

Lythe, M. B., Vaughan, D. G. & BEDMAP CONSORTIUM 2001. BEDMAP: a new thickness and subglacial topographic model of Antarctica. *Journal of Geophysical Research*, **106**, 11335–11351.

Macdonald, F. A. 2011. The Tsagaan Oloom Formation, southwestern Mongolia. *In*: Arnaud, E., Halverson, G. P. & Shields, G. (eds) *The Geological Record of Neoproterozoic Glaciations*. Geological Society, London, Memoirs, **36**, 331–337.

Macdonald, F. A. & Cohen, P. A. 2011. The Tatonduk inlier, Alaska–Yukon border. *In*: Arnaud, E., Halverson, G. P. & Shields, G. (eds) *The Geological Record of Neoproterozoic Glaciations*. Geological Society, London, Memoirs, **36**, 389–396.

Macdonald, F. A. & Jones, D. S. 2011. The Khubsugul Group, northern Mongolia. *In*: Arnaud, E., Halverson, G. P. & Shields, G. (eds) *The Geological Record of Neoproterozoic Glaciations*. Geological Society, London, Memoirs, **36**, 339–345.

Macdonald, F. A., Mcclelland, W. C., Schrag, D. P. & Macdonald, W. P. 2009. Neoproterozoic glaciation on a carbonate platform margin in Arctic Alaska and the origin of the North Slope subterrane. *Geological Society of America Bulletin*, **121**, 448–473.

Macdonald, F. A., Schmidtz, M. D. *et al.* 2010. Calibrating the Cryogenian. *Science*, **327**, 1241–1243.

Macdonald, F. A., Strauss, J. V., Rose, C., Dudás, F. Ö. & Schrag, D. P. 2011. Stratigraphy of the Port Nolloth Group of Namibia and South Africa and implications for the age of Neoproterozoic iron formations. *American Journal of Science*, **310**, 862–888.

Martin, H. 1965*a*. The Precambrian Geology of South West Africa and Namaqualand. *University of Cape Town, Precambrian Research Unit Bulletin*, **1**, 1–159.

Martin, H. 1965*b*. *Beobachtungen zum Problem der jung-präkambrischen Glazialen Ablagerungen in Südwestafrika* (Observations concerning the problem of the late Precambrian glacial deposits in South West Africa). *Geologische Rundschau*, **54**, 115–127.

Mikucki, J. A., Pearson, A. *et al.* 2009. A contemporary microbially maintained subglacial ferrous 'ocean'. *Science*, **324**, 397–400.

Moore, T. S., Murray, R. W., Kurtz, A. C. & Schrag, D. P. 2004. Anaerobic methane oxidation and the formation of dolomite. *Earth and Planetary Science Letters*, **229**, 141–154.

Myrow, P. M. & Kaufman, A. J. 1999. A newly discovered cap carbonate above Varanger-age glacial deposits in Newfoundland, Canada. *Journal of Sedimentary Research*, **69**, 784–793.

Nédélec, A., Affaton, P., France-Lanord, C., Charrière, A. & Alvaro, J. 2007. Sedimentology and chemostratigraphy of the Bwipe Neoproterozoic cap dolostones (Ghana, Volta Basin): a record of microbial activity in a peritidal environment. *C. R. Geoscience*, **339**, 223–239.

Nogueira, A. C. R., Riccomini, C., Sial, A. N., Moura, C. A. V. & Fairchild, T. R. 2003. Soft-sediment deformation at the base of the Neoproterozoic Puga cap carbonate (southwestern Amazon craton, Brazil): confirmation of rapid icehouse to greenhouse transition in snowball Earth. *Geology*, **31**, 613–616.

Nogueira, A. C. R., Riccomini, C., Sial, A. N., Moura, C. A. V., Trindade, R. I. F. & Fairchild, T. R. 2007. Carbon and strontium isotope fluctuations and paleoceanographic changes in late Neoproterozoic Araras carbonate platform, southern Amazon craton, Brazil. *Chemical Geology*, **237**, 168–190.

Pierrehumbert, R. T. 2002. The hydrologic cycle in deep-time climate problems. *Nature*, **419**, 191–198.

Plummer, P. S. 1978. Note on the palaeoenvironmental significance of the Nuccaleena Formation (upper Precambrian), central Flinders Ranges, South Australia. *Journal of the Geological Society of Australia*, **25**, 395–402.

Prave, A. R., Hoffmann, K.-H., Hegenberger, W. & Fallick, A. E. 2011. The Witvlei Group of east-central Namibia. *In*: Arnaud, E., Halverson, G. P. & Shields, G. (eds) *The Geological Record of Neoproterozoic Glaciations*. Geological Society, London, Memoirs, **36**, 211–216.

Preiss, W. V. 1987. The Adelaide Geosyncline: Late Proterozoic stratigraphy, sedimentation, palaeontology and tectonics. *Geological Survey of South Australia Bulletin*, **53**, 438.

Preiss, W. V., Walter, M. R., Coates, R. P. & Wills, A. T. 1978. Lithological correlation of the Adelaidean glaciogenic rocks in parts of the Amadeus, Ngalia & Georgina basins. *Bureau of Mineral Resources, Journal of Australian Geology and Geophysics*, **3**, 43–53.

Pruss, S. B., Bosak, T., Macdonald, F. A., Mclane, M. & Hoffman, P. F. 2010. Microbial facies in a Sturtian cap carbonate, the Rasthof Formation, Otavi Group, northern Namibia. *Precambrian Research*, **181**, 187–108.

Rankama, K. 1973. The Late Precambrian glaciation, with particular reference to the Southern Hemisphere. *Journal and Proceedings, Royal Society of New South Wales*, **106**, 89–97.

Raub, T. D. 2008. *Prolonged deglaciation of 'Snowball Earth'*. PhD thesis, Yale University, CT.

Ridgwell, A. J., Kennedy, M. J. & Caldeira, K. 2003. Carbonate deposition, climate stability and Neoproterozoic ice ages. *Science*, **302**, 859–862.

Roberts, A. P. 2008. Geomagnetic excursions: knowns and unknowns. *Geophysical Research Letters*, **35**, L17307, doi: 10.1029/2008GL034719.

Roberts, A. P. & Lewin-Harris, J. C. 2000. Marine magnetic anomalies: evidence that 'tiny wiggles' represent short-period geomagnetic polarity intervals. *Earth and Planetary Science Letters*, **183**, 375–388.

Sheldon, R. P. 1984. Ice-ring origin of the Earth's atmosphere and hydrosphere and Late Proterozoic–Cambrian hypothesis. *Geological Survey of India Special Publication*, **17**, 17–21.

Shields, G. A. 2005. Neoproterozoic cap carbonates: a critical appraisal of existing models and the plumeworld hypothesis. *Terra Nova*, **17**, 299–310.

Shields, G. A., Deynoux, M., Strauss, H., Paquet, H. & Nahon, D. 2007. Barite-bearing cap dolostone of the Taoudéni Basin, northwest Africa: sedimentary and isotopic evidence for methane seepage after a Neoproterozoic glaciation. *Precambrian Research*, **154**, 209–235.

Smith, L. H., Kaufman, A. J., Knoll, A. H. & Link, P. K. 1994. Chemostratigraphy of predominantly siliciclastic Neoproterozoic successions: a case study of the Pocatello Formation and lower Brigham Group, Idaho. *Geological Magazine*, **131**, 301–314.

Sovetov, Yu. K. & Komlev, D. A. 2005. Tillites at the base of the Oselok Group, foothills of the Sayan Mountains, and the Vendian lower boundary in the southwestern Siberian Platform. *Stratigraphy and Geological Correlations*, **13**, 337–366.

Sumner, D. Y. 2002. Decimetre-thick encrustations of calcite and aragonite on the sea-floor and implications for Neoarchaean and Neoproterozoic ocean chemistry. *Special Publications of the International Association of Sedimentologists*, **33**, 107–120.

Tojo, B., Katsuta, N., Takano, M., Kawakami, S. & Ohno, T. 2007. Calcite–dolomite cycles in the Neoproterozoic Cap carbonates, Otavi Group, Namibia. *In*: Vickers-Rich, P. & Komarower, P. (eds) *The Rise and Fall of the Ediacaran Biota*. Geological Society, London, Special Publication, **286**, 103–113.

Trindade, R. I. F., Font, E., D'agrella-Filho, M. S., Nogueira, A. C. R. & Riccimini, C. 2003. Low-latitude and multiple geomagnetic reversals in the Neoproterozoic Puga cap carbonate, Amazon craton. *Terra Nova*, **15**, 441–446.

Trompette, R. 1994. *Geology of Western Gondwana (2000–500 Ma): Pan-African–Brasiliano Aggregation of South America and Africa*. Balkema, Amsterdam.

Trompette, R., Affaton, P., Joulia, F. & Marchand, J. 1980. Stratigraphic and structural controls of late Precambrian phosphate deposits of the Northern Volta Basin in Upper Volta, Niger and Benin, West Africa. *Economic Geology*, **75**, 62–70.

Trompette, R., de Alvarenga, C. J. A. & Wade, D. 1998. Geological evolution of the Neoproterozoicv Corumbá graben system (Brazil). Depositional context of the stratified Fe and Mn ores of the Jacadigo Group. *Journal of South American Earth Sciences*, **11**, 587–597.

Urban, H., Stribny, B. & Lippolt, H. J. 1992. Iron and manganese deposits of the Urucum District, Mato Grosso do Sul, Brazil. *Economic Geology*, **87**, 1375–1892.

van Lith, Y., Warthmann, R., Vasconcelos, C. & McKenzie, J. A. 2003. Sulphate-reducing bacteria induce low-temperature Ca-dolomite and high Mg-calcite formation. *Geobiology*, **1**, 71–79.

Walde, D. H. G., Gierth, E. & Leonardos, O. H. 1981. Stratigraphy and mineralogy of the manganese ores of Urucum, Mato Grosso, Brazil. *Geologische Rundschau*, **70**, 1077–1085.

Wallace, J. M. & Hobbs, P. V. 1977. *Atmospheric Science: An Introductory Survey*. Academic Press, San Diego.

Walter, M. R. & Bauld, J. 1983. The association of sulphate evaporites, stromatolitic carbonates and glacial sediments: examples from the Proterozoic of Australia and the Cainozoic of Antarctic. *Precambrian Research*, **21**, 129–148.

Wang, J., Jiang, G., Xiao, S., Li, Q. & Wei, Q. 2008. Carbon isotope evidence for widespread methane seeps in the ca 635 Ma Doushantuo cap carbonate in South China. *Geology*, **36**, 347–350.

Warren, S. G., Brandt, R. E., Grenfell, T. C. & Mckay, C. P. 2002. Snowball Earth: ice thickness on the tropical ocean. *Journal of Geophysical Research*, **107**, 3167, doi: 10.1029/2001JC001123.

Whitten, G. F. 1970. The investigation and exploitation of the Razorback Ridge iron deposit. *Geological Survey of South Australia Reports of Investigations*, **33**, 165.

Xiao, S., Bao, H. *et al.* 2004. The Neoproterozoic Quruqtagh Group in eastern Chinese Tianshan: evidence for a post-Marinoan glaciation. *Precambrian Research*, **130**, 1–26.

Yeo, G. M. 1981. The Late Proterozoic Rapitan glaciation in the northern Cordillera. *In*: Campbell, F. H. A. (ed.) *Proterozoic Basins of Canada*. Geological Survey of Canada Paper, **81–10**, 25–46.

Yeo, G. M. 1986. Iron-formation in the late Proterozoic Rapitan Group, Yukon and Northwest Territories. *In*: Morin, J. A. (ed.) *Mineral Deposits of Northern Cordillera*. Canadian Institute of Mining and Metallurgy Special Volume, **37**, 142–153.

Young, G. M. 1976. Iron-formation and glaciogenic rocks of the Rapitan Group, Northwest Territories, Canada. *Precambrian Research*, **3**, 137–158.

Zhang, S., Jiang, G. & Han, Y. 2008. The age of the Nantuo Formation and Nantuo glaciation in South China. *Terra Nova*, **20**, 289–294.

Zhou, C., Bao, H., Peng, Y. & Yuan, X. 2010. Timing of deposition of ^{17}O-depleted barite at the Nantuo glacial meltdown in South China. *Geology*, **38**, 903–906.